Received 2005 April 21; Accepted 2005 July 7
Preprint typeset using LaTeX style emulateapj v. 11/26/03

A CENSUS OF OPTICAL AND NEAR-INFRARED SELECTED STAR-FORMING AND PASSIVELY EVOLVING GALAXIES AT REDSHIFT $Z \sim 2$[1]

Naveen A. Reddy, Dawn K. Erb, Charles C. Steidel
California Institute of Technology, MS 105–24, Pasadena, CA 91125

Alice E. Shapley[2]
Astronomy Department, University of California, Berkeley, 601 Campbell Hall, Berkeley, CA 94720

Kurt L. Adelberger[3]
Observatories of the Carnegie Institution of Washington, 813 Santa Barbara Street, Pasadena, CA 91101

and

Max Pettini
Institute of Astronomy, Madingley Road, Cambridge CB3 OHA, UK
Received 2005 April 21; Accepted 2005 July 7

ABSTRACT

Using the extensive multi-wavelength data in the GOODS-North field, including our ground-based rest-frame UV spectroscopy and near-IR imaging, we construct and draw comparisons between samples of optical and near-IR selected star-forming and passively evolving galaxies at redshifts $1.4 \lesssim z \lesssim 2.6$. We find overlap at the $70-80\%$ level in samples of $z \sim 2$ star-forming galaxies selected by their optical ($U_{\rm n}G\mathcal{R}$) and near-IR (BzK) colors when subjected to common K-band limits. Deep *Chandra* data indicate a $\sim 25\%$ AGN fraction among near-IR selected objects, much of which occurs among near-IR bright objects ($K_{\rm s} < 20$; Vega). Using X-rays as a proxy for bolometric star formation rate (SFR) and stacking the X-ray emission for the remaining (non-AGN) galaxies, we find the SFR distributions of $U_{\rm n}G\mathcal{R}$, BzK, and $J-K_{\rm s} > 2.3$ galaxies (i.e., Distant Red Galaxies; DRGs) are very similar as a function of $K_{\rm s}$, with $K_{\rm s} < 20$ galaxies having $\langle SFR \rangle \sim 120$ M$_\odot$ yr^{-1}, a factor of two to three higher than those with $K_{\rm s} > 20.5$. The absence of X-ray emission from the reddest DRGs and BzK galaxies with $(z-K)_{\rm AB} \gtrsim 3$ indicates they must have declining star formation histories to explain their red colors and low SFRs. While the M/L ratio of passively-evolving galaxies may be larger on average, the *Spitzer*/IRAC data indicate that their inferred stellar masses do not exceed the range spanned by optically selected galaxies, suggesting that the disparity in current SFR may not indicate a fundamental difference between optical and near-IR selected massive galaxies ($M^* > 10^{11}$ M$_\odot$). We consider the contribution of optical, near-IR, and submillimeter-selected galaxies to the star formation rate density (SFRD) at $z \sim 2$, taking into account sample overlap. The SFRD in the interval $1.4 \lesssim z \lesssim 2.6$ of $U_{\rm n}G\mathcal{R}$ and BzK galaxies to $K_{\rm s} = 22$, and DRGs to $K_{\rm s} = 21$ is $\sim 0.10 \pm 0.02$ M$_\odot$ yr^{-1} Mpc^{-3}. Optically-selected galaxies to $\mathcal{R} = 25.5$ and $K_{\rm s} = 22.0$ account for $\sim 70\%$ of this total. Greater than 80% of radio-selected submillimeter galaxies to $S_{850\mu{\rm m}} \sim 4$ mJy with redshifts $1.4 < z < 2.6$ satisfy either one or more of the BX/BM, BzK, and DRG criteria.

Subject headings: cosmology: observations — galaxies: evolution — galaxies: high redshift — galaxies: starburst — infrared: galaxies — X-rays: galaxies

1. INTRODUCTION

A number of surveys have been developed to select galaxies at $z \sim 2$, determine their bolometric star formation rates (SFRs), and compare with other multi-wavelength studies to form a census of the total star formation rate density (SFRD) at $z \sim 2$ (e.g., Steidel et al. 2004; Rubin et al. 2004; Daddi et al. 2004b). A parallel line of study has been to compare optical and near-IR selected galaxies that are the plausible progenitors of the local population of passively evolving massive galaxies. However, biases inherent in surveys that select galaxies based on their star formation activity (e.g., Steidel et al. 2004) and stellar mass (e.g., Cimatti et al. 2002b; Glazebrook et al. 2004) can complicate such comparisons. Only with an accurate knowledge of the overlap between these samples can we begin to address the associations between galaxies selected in different ways, their mutual contribution to the SFRD at $z \sim 2$, and the prevalence and properties of passively evolving and massive galaxies at high redshift. Quantifying this overlap between optical and near-IR surveys is a primary goal of this paper.

In practice, optical surveys are designed to *efficiently* select galaxies with a specific range of properties. The imaging required for optical selection is generally a small fraction of the time required for near-IR imaging, and can cover much larger areas within that time. In contrast,

[1] Based, in part, on data obtained at the W.M. Keck Observatory, which is operated as a scientific partnership among the California Institute of Technology, the University of California, and NASA, and was made possible by the generous financial support of the W.M. Keck Foundation.
[2] Miller Fellow
[3] Carnegie Fellow

near-IR surveys sample galaxies over a wider baseline in wavelength than optical surveys, and can include galaxies relevant to studying both the star formation rate and stellar mass densities at high redshift. However, in order to achieve a depth similar (and area comparable) to that of optical surveys, near-IR selection requires extremely deep imaging and can be quite expensive in terms of telescope time due to the relatively small size of IR arrays compared to CCDs. Furthermore, the "color" of the terrestrial background for imaging is $(B-K_{\rm s})_{\rm AB} \simeq 7$ magnitudes, much redder than all but the most extreme $z \sim 2$ galaxies. Once selected, of course, such extreme galaxies then require heroic efforts to obtain spectra, whereas optical selection, particularly at redshifts where key features fall shortward of the bright OH emission "forest", virtually guarantees that one can obtain a spectroscopic redshift with a modest investment of 8-10m telescope time and a spectrograph with reasonably high throughput. As we show below, optical and near-IR surveys complement each other in a way that is necessary for obtaining a reasonably complete census of galaxies at high redshift.

The SFRs of $z \sim 2$ galaxies are typically estimated by employing locally-calibrated relations between emission at which the galaxies can be easily detected (e.g., UV, Hα) and their FIR emission. The X-ray luminosity of local non-active galaxies results primarily from high mass X-ray binaries, supernovae, and diffuse hot gas (e.g., Grimm et al. 2002; Strickland et al. 2004); all of these sources of X-ray emission are related to the star formation activity on timescales of $\lesssim 100$ Myr. Observations of galaxies in the local universe show a tight correlation between X-ray and FIR luminosity, prompting the use of X-ray emission as an SFR indicator (Ranalli et al. 2003). This correlation between X-ray emission and SFR applies to galaxies with a very large range in SFRs, from $\sim 0.1-1000\,{\rm M}_{\odot}\,{\rm yr}^{-1}$. Stacking analyses at X-ray and radio wavelengths, and comparison with UV emission, indicate that the local SFR relations appear to give comparable estimates of the instantaneous SFRs of galaxies after assuming continuous star formation models and correcting for dust (e.g., Reddy & Steidel 2004; Nandra et al. 2002; Seibert et al. 2002).

Two surveys designed to select massive galaxies at redshifts $1.4 \lesssim z \lesssim 2.5$ and passively-evolving (PE) galaxies at redshifts $z \gtrsim 2$, respectively, are the K20 and FIRES surveys. The K20 and FIRES selection criteria were developed to take advantage of the sensitivity of rest-frame optical light and color to stellar mass and the strength of the Balmer break, respectively, for $z \sim 2$ galaxies (e.g., Cimatti et al. 2002a; Franx et al. 2003). The Gemini Deep Deep Survey (GDDS) extends this near-IR technique to target massive galaxies at slightly lower redshifts ($0.8 \lesssim z \lesssim 2.0$; Abraham et al. 2004).

X-ray stacking analyses of the brightest galaxies in the K20 and FIRES surveys indicate an average SFR a factor of 4 to 5 times larger than for optically-selected $z \sim 2$ galaxies (Daddi et al. 2004a; Rubin et al. 2004), inviting the conclusion that optical selection misses a large fraction of the star formation density at high redshift. While it is certainly true that optical surveys miss some fraction of the SFRD, the past quoted difference in the average SFRs of galaxies selected optically and in the near-IR disappears once the galaxies are subjected to a common near-IR magnitude limit, as we show below.

We have recently concluded a campaign to obtain deep near-IR imaging for fields in the $z \sim 2$ optical survey (Steidel et al. 2004), allowing for a direct comparison of optical and near-IR selected galaxies. One result of this comparison is that $K_{\rm s} < 20$ (Vega) optically-selected galaxies show similar space densities, stellar masses, and metallicities as $K_{\rm s}$-bright galaxies in near-IR samples (Shapley et al. 2004). More recently, Adelberger et al. (2005) show that the correlation lengths for $K_{\rm s}$-bright galaxies among optical and near-IR samples are similar, suggesting an overlap between the two sets of galaxies, both of which plausibly host the progenitors of massive elliptical galaxies in the local universe. These results suggest that near-IR bright galaxies have similar properties regardless of the method used to select them.

In this paper, we extend these results by examining the color distributions and X-ray properties of near-IR and optically selected galaxies at $z \sim 2$ in the GOODS-North field (Giavalisco et al. 2004). The field is well-suited for this analysis given the wealth of complementary data available, including *Chandra*/X-ray, ground-based optical and near-IR, and *Spitzer*/IRAC imaging. Multi-wavelength data in a single field are particularly useful in that we can use a common method for extracting photometry that is not subject to the biases that may exist when comparing galaxies in different fields whose fluxes are derived in different ways. The addition of our rest-frame UV spectroscopic data in the GOODS-N field provides for a more detailed analysis than otherwise possible of the properties of galaxies as a function of selection technique. Furthermore, the GOODS-N field coincides with the *Chandra* Deep Field North (CDF-N) region which have the deepest (2 Ms) X-ray data available (Alexander et al. 2003). The X-ray data allow for an independent estimate of bolometric SFRs and the available depth allows more leeway in stacking smaller numbers of sources to obtain a statistical detection, as well as identifying AGN to a lower luminosity threshold than possible in other fields that have shallower X-ray data.

The outline of the paper is as follows. In §2, we describe the optical, near-IR, X-ray, and IRAC data and present the optical and near-IR selection criteria and X-ray stacking method. Color distributions, direct X-ray detections, and stacked results are examined in §3. In §4, we discuss the SFR distributions of optical and near-IR selected $z \sim 2$ galaxies and their relative contributions to the SFRD, and the presence of a passively evolving population of galaxies. A flat ΛCDM cosmology is assumed with $H_0 = 70$ km s^{-1} Mpc^{-1} and $\Omega_{\Lambda} = 0.7$.

2. DATA AND SAMPLE SELECTION

2.1. *Imaging*

Optical $U_{\rm n}G\mathcal{R}$ images in the GOODS-North field were obtained in 2002 and 2003 April under photometric conditions using the KPNO and Keck I telescopes. The KPNO/MOSAIC U-band image was obtained from the GOODS team (PI: Giavalisco) and was transformed to reflect $U_{\rm n}$ magnitudes (e.g., Steidel et al. 2004). The Keck I G and $\mathcal{R}$ band images were taken by us with the Low Resolution Imaging Spectrograph (LRIS; Oke et al. 1995, Steidel et al. 2004), and were oriented to provide the maximum overlap with the GOODS ACS and *Spitzer* survey region. The images cover $11' \times 15'$ with FWHM

Table 1. Interloper Contamination of the BX/BM Sample

K_s Range	N_{phot}[a]	N_{spec}[b]	$N_{z<1}$[c]	$f_{z<1}$[d]
$K_s \leq 20.0$	61	18	7	0.39
$20.0 < K_s \leq 20.5$	58	23	2	0.09
$20.5 < K_s \leq 21.0$	82	30	3	0.10
$21.0 < K_s \leq 21.5$	101	32	2	0.06
$21.5 < K_s \leq 22.0$	141	29	3	0.10

[a]Number of photometric BX/BM candidates.
[b]Number of candidates with spectroscopic redshifts.
[c]Number of interlopers.
[d]Interloper fraction.

$\sim 0\farcs7$ to a depth of $\mathcal{R} \sim 27.5$ ($3\,\sigma$). Image reduction and photometry were done following the procedures described in Steidel et al. (2003). We obtained deep B-band images of the GOODS-N field from a public distribution of *Subaru* data (Capak et al. 2004). The deep z-band data are acquired from the public distribution of the *HST* Advanced Camera for Surveys (ACS) data (Giavalisco et al. 2004). The B and z band data have $5\,\sigma$ depth of 26.9 and 27.4 mag measured in 3 $''$ and $0\farcs2$ diameter apertures, respectively. The K_s and J imaging was accomplished with the Wide Field Infrared Camera (WIRC) on the Palomar Hale 5 m telescope (Wilson et al. 2003), providing $8\farcm7 \times 8\farcm7$ coverage in the central portion of the GOODS-N field. The near-IR images cover $\sim 43\%$ of the optical image. The images had FWHM $\sim 1\farcs0$ under photometric conditions and $3\,\sigma$ sensitivity limits of ~ 22.6 and ~ 24.1 mag in the K_s and J bands, respectively. The near-IR data are described in detail by Erb et al. (2005). The total area studied in the subsequent analysis is ~ 72.3 arcmin^2.

The procedures for source detection and photometry are described in Steidel et al. (2003). Briefly, $U_nG\mathcal{R}$ magnitudes were calculated assuming isophotal apertures that were adjusted to the $\mathcal{R}$-band flux profiles. Source detection was done at K_s-band. BzK and J magnitudes are computed assuming the isophotal apertures adjusted to the K_s-band flux profiles, unless the $\mathcal{R}$-band isophotes gave a more significant K_s detection. In the analysis to follow, "K_s" and J magnitudes are in Vega units. We use the conversion $K_{AB} = K_s + 1.82$. All other magnitudes are in AB units.

Fully reduced *Spitzer*/IRAC mosaics of the GOODS-North field were made public in the first data release of the GOODS Legacy project (PI: Dickinson). The IRAC data overlap completely with our K_s-band image, but currently only two channels (either 3.6 μm and 5.8 μm, or 4.5 μm and 8.0 μm) are available over most of the image. A small area of overlap has coverage in all four channels. The images are deep enough that source confusion is an issue. We have mitigated the effects of confusion noise by employing the higher spatial resolution K_s-band data to constrain source positions and deblend confused IRAC sources. We performed PSF photometry using the procedure described in Shapley et al. (2005).

2.2. *Selection Criteria*

Optical Selection of Star-Forming Galaxies

We have optically-selected $z \sim 2$ galaxies in the GOODS-N field based on their observed $U_nG\mathcal{R}$ colors (Adelberger et al. 2004; Steidel et al. 2004) to a limiting magnitude of $\mathcal{R} = 25.5$. The selection criteria aim to select actively star forming galaxies at $z \sim 2$ with the same range in UV properties and extinction as LBGs at $z \sim 3$ (Steidel et al. 2003). "BX" galaxies are selected to be at redshifts $2.0 \lesssim z \lesssim 2.6$ using the following criteria:

$$\begin{aligned} G - \mathcal{R} &\geq -0.2 \\ U_n - G &\geq G - \mathcal{R} + 0.2 \\ G - \mathcal{R} &\leq 0.2(U_n - G) + 0.4 \\ U_n - G &\leq G - \mathcal{R} + 1.0, \end{aligned} \quad (1)$$

and "BM" objects are selected to be at redshifts $1.5 \lesssim z \lesssim 2.0$ using the following criteria:

$$\begin{aligned} G - \mathcal{R} &\geq -0.2 \\ U_n - G &\geq G - \mathcal{R} - 0.1 \\ G - \mathcal{R} &\leq 0.2(U_n - G) + 0.4 \\ U_n - G &\leq G - \mathcal{R} + 0.2 \end{aligned} \quad (2)$$

(Adelberger et al. 2004; Steidel et al. 2004). For subsequent analysis, we will refer to BX and BM objects as those which are optically-, or "BX/BM"-, selected.

Optical color selection of $z \sim 2$ galaxies in the $11'$ by $15'$ area of the GOODS-North field yielded 1360 BX and BM candidates, of which 620 lie in the region where we have complementary J and K-band data (§ 2.1), and 199 have $K_s < 21.0$. Followup spectroscopy with the blue channel of the Low Resolution Imaging Spectrograph (LRIS-B) yielded 147 redshifts for objects with K_s-band data (248 redshifts over the entire optical field). Of these 147 objects with redshifts and K_s-band data, 129 have $z > 1$, and 60 have $z > 1$ *and* $K_s < 21$. The mean redshift of the 60 BX/BM objects is $\langle z \rangle = 1.99 \pm 0.36$. The spectroscopic interloper fractions in the BX/BM sample are summarized in Table 1. The BX and BM selection functions (shown as shaded distributions in Figure 1) have distributions with mean redshifts $\langle z \rangle = 2.2 \pm 0.3$ and $\langle z \rangle = 1.7 \pm 0.3$, respectively (Steidel et al. 2004), and the combination of these two samples comprise our BX/BM-selected $z \sim 2$ sample. In the analysis to follow, we designate an interloper as any object with $z < 1$.

Near-IR Selection of Star-Forming Galaxies

The near-IR properties of galaxies can be used both to target star forming galaxies and to identify those with

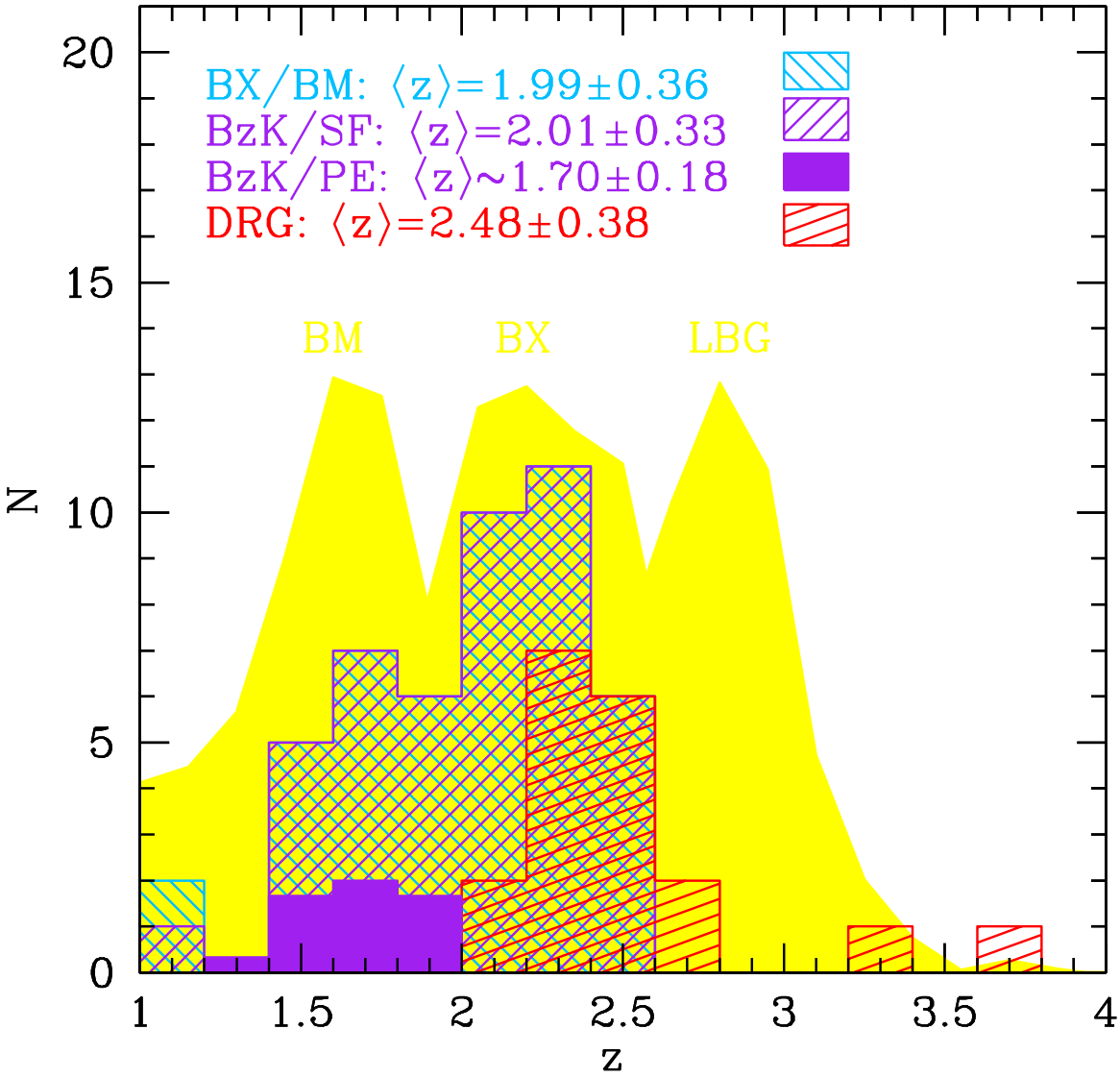

FIG. 1.— *Spectroscopic* redshift distributions to $K_s = 21$ for the various samples considered here. The BX/BM and BzK/SF distributions (hashed histograms) include sources from our sample in the GOODS-North field and overlap almost completely. The DRGs have a higher mean redshift of $\langle z \rangle = 2.48 \pm 0.38$ from our sample of $J - K_s > 2.3$ sources with $z > 1$ in all four fields of the optical survey (Steidel et al. 2004) where we have complementary J and K-band imaging. The redshift distribution of DRGs within our sample (all of which are selected with the BX/BM or $z \sim 3$ LBG criteria) is similar to that found by van Dokkum et al. (2004), van Dokkum et al. (2003), and Förster Schreiber et al. (2004). The solid histogram shows the redshift distribution for BzK/PE galaxies from Daddi et al. (2004a) and Daddi et al. (2005), scaled down by a factor of 3 for clarity. The background shaded regions show the arbitrarily normalized redshift distributions for optically-selected BX and BM galaxies, and LBGs.

extremely red colors which may indicate passive evolution. To address the former issue, we have employed the "BzK" selection criteria of Daddi et al. (2004a) to cull objects in the GOODS-N field and directly compare with those selected on the observed optical properties of $z \gtrsim 2$ galaxies. Daddi et al. (2004a) define the quantity "BzK":

$$BzK \equiv (z - K) - (B - z); \quad (3)$$

star-forming galaxies with $z > 1.4$ are targeted by the following criterion:

$$BzK \geq -0.2, \quad (4)$$

in AB magnitudes. Of the 1185 sources with $> 3\,\sigma$ B, z, and K detections and $K_s < 21$, 221 satisfy Equation 4. The surface density of BzK galaxies with $K_s < 21$ is ~ 3 arcmin^{-2}, similar to the surface density of BX/BM galaxies to a similar K_s-band depth. These star-forming BzK galaxies will be referred to as "BzK/SF" galaxies, and their spectroscopic redshift distribution *from our spectroscopic sample* is shown in Figure 1. Our deep near-IR imaging allows us to determine the redshift distribution for BzK/SF galaxies with $K_s > 20$ (and which also satisfy the BX/BM criteria), and the results are shown in Figure 2. The mean redshifts of the $K_s \leq 20$ and $K_s > 20$ distributions are $\langle z \rangle = 2.13 \pm 0.22$ and $\langle z \rangle = 2.03 \pm 0.41$, respectively, and agree within the uncertainty. We note, however, that the BzK/SF criteria select $K_s > 20$ objects over a broader range in redshift ($1.0 \leq z \leq 3.2$) than $K_s \leq 20$ objects. This reflects the larger range in BzK colors of $K_s > 20$ BzK/SF galaxies compared with those having $K_s \leq 20$. Additionally, the photometric scatter

in colors is expected to increase for fainter objects, so a broadening of the redshift distribution for BzK/SF objects with fainter K_s magnitudes is not surprising.

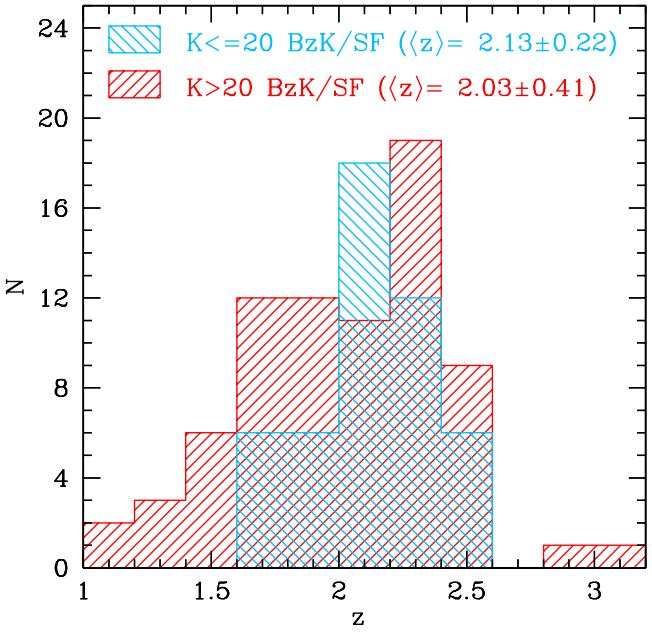

FIG. 2.— Arbitrarily normalized spectroscopic redshift distribution of BzK/SF galaxies in our spectroscopic sample to $K_s \sim 22.5$, with separate emphasis on $K_s \leq 20$ and $K_s > 20$ BzK/SF objects. The BzK/SF criteria select $K_s > 20$ objects over a broader range in redshift than $K_s \leq 20$ objects.

We emphasize that we only know the redshifts for BzK/SF galaxies which also happen to fall in the BX/BM sample. In general, the true redshift distribution, $N_o^{BzK/SF}(z)$, of the BzK/SF sample will be broader than the distributions shown in Figure 1 and Figure 2, call them $N_c^{BzK/SF}(z)$), which are effectively convolved with the BX/BM selection function. For example, the rapid dropoff in $N_c^{BzK/SF}(z)$ for $z > 2.6$ (Figure 2) may simply reflect the dropoff in the BX selection function for $z > 2.6$. However, the $N_c^{BzK/SF}(z)$ we derive here is similar to that of the *photometric* redshift distribution of K20 galaxies from Daddi et al. (2004a), which is subject to its own systematic errors, suggesting that a reasonable approximation is to take $N_o^{BzK/SF}(z) \simeq N_c^{BzK/SF}(z)$.

Near-IR Selection of Passively Evolving Galaxies

In addition to the criteria above, several methods have been developed to select passively evolving high redshift galaxies by exploiting the presence of absorption or continuum breaks in the SEDs of galaxies with dominant old stellar populations. The BzK selection criteria

$$BzK < -0.2$$
$$z - K > 2.5 \quad (5)$$

are designed to select passively evolving galaxies at $z > 1.4$ (Cimatti et al. 2004; Daddi et al. 2004a). One galaxy which has a secure B-band detection, and an additional 16 with B-band limits, satisfy these criteria, implying a surface density of BzK/PE galaxies of 0.24 arcmin^{-2} to $K_s = 21$. Galaxies selected by their BzK colors to be passively-evolving are referred to as "BzK/PE" objects. The redshift distribution of BzK/PE galaxies, taken from the spectroscopic samples of Daddi et al. (2004a) and Daddi et al. (2005), shows that they mostly lie between redshifts $1.4 \lesssim z \lesssim 2$ (Figure 1). We note that

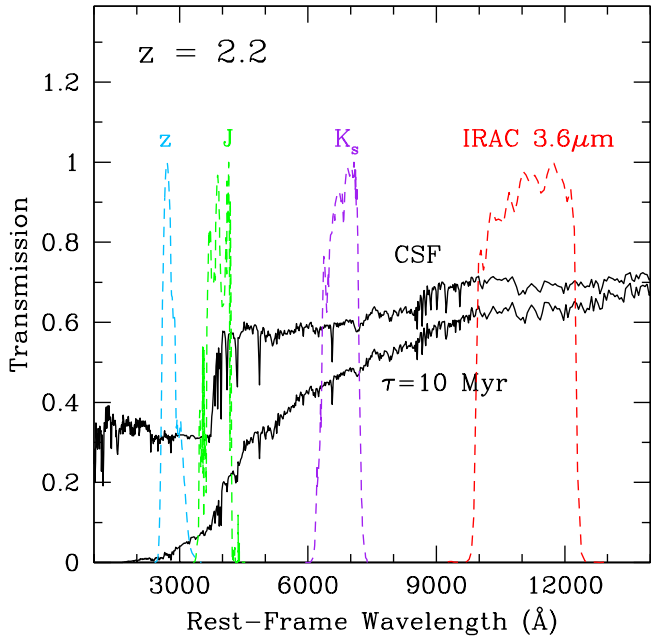

FIG. 3.— Relative transmission of the z, J, K_s, and IRAC 3.6 μm filters at rest-frame wavelengths for $z = 2.2$. Also shown are typical (unreddened) galaxy SEDs assuming constant star formation (CSF) and instantaneous star formation ($\tau = 10$ Myr) aged to 1 Gyr. For redshifts $z \sim 1.88 - 2.38$, the J-band brackets the prominent Balmer and 4000 Å breaks.

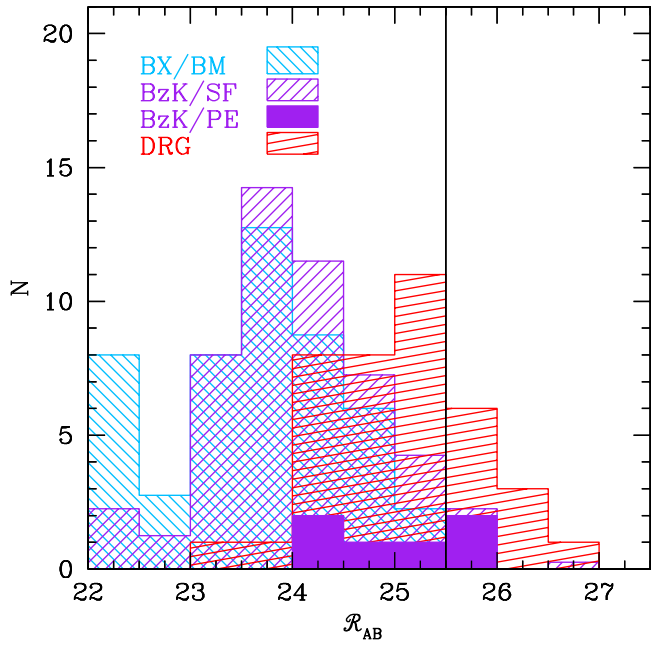

FIG. 4.— Optical magnitude distributions for photometrically selected $K_s < 21$ galaxies in the BX/BM, BzK, and DRG samples. The solid vertical line denotes the magnitude limit for galaxies in the optically-selected (BX/BM) sample. Approximately 47% of DRGs (34/73) have $\mathcal{R} > 27.0$ and are not shown in the figure. The distribution of BzK/PE galaxies has been arbitrarily normalized for clarity.

Table 2. Sample Properties

K_s Range	Sample	N_T[a]	N_X[b]	N_S[c]	$\langle z \rangle$[d]	$\langle L_{2.0-10\,keV} \rangle$ ($\times 10^{41}$ ergs s^{-1})	$\langle SFR_x \rangle$ ($M_\odot$ yr^{-1})
$18.0 < K_s \leq 20.0$	BX/BM[e]	11	4	10 (7)	1.75 (1.80)	7.13 ± 0.88 (4.95 ± 1.15)	143 (99)
	BzK/SF	77	24	45 (42)	1.97 (2.01)	5.39 ± 0.46 (4.68 ± 0.48)	108 (94)
	BzK/PE	14	3	11	1.74	3.07 ± 0.84	61
	DRG	20	5	14	2.48	5.26 ± 1.28	105
$20.0 < K_s \leq 20.5$	BX/BM [e]	21	0	21	2.03	4.89 ± 0.79	98
	BzK/SF	57	5	56 (55)	2.01 (2.01)	3.96 ± 0.40 (3.87 ± 0.41)	79 (77)
	BzK/PE	0	0	...	...	...	...
	DRG	20	7	13	2.48	2.32 ± 1.30	46
$20.5 < K_s \leq 21.0$	BX/BM [e]	27	0	27	1.99	2.11 ± 0.56	42
	BzK/SF	87	3	82 (81)	2.01 (2.01)	2.32 ± 0.30 (2.20 ± 0.30)	46 (44)
	BzK/PE	3	1	2	1.74	2.07 ± 1.54	41
	DRG	33	7	26	2.48	1.90 ± 0.86	38
$21.0 < K_s \leq 21.5$	BX/BM [e]	31	0	31	2.04	2.95 ± 1.01	59
	BzK/SF	99	2	97	2.01	2.76 ± 0.28	55
$21.5 < K_s \leq 22.0$	BX/BM [e]	26	0	26	2.22	1.43 ± 0.77	29
	BzK/SF	148	0	148	2.01	2.78 ± 0.73	56
$22.0 < K_s \leq 22.5$	BX/BM [f]	93	0	93	2.04	1.13 ± 0.25	23
	BzK/SF	77	0	77	2.01	0.49 ± 0.29	10

[*]Note.—Values in parentheses are when we exclude all directly-detected X-ray sources, including ones which may be star-forming galaxies (Table 3).
[a]Total number of sources in sample.
[b]Number of direct X-ray detections, corresponding to a minimum 3 σ flux of $f_{0.5-2.0\ keV} \sim 2.5 \times 10^{-17}$ erg s^{-1} cm^{-2}.
[c]Number of stacked sources.
[d]Mean redshift of stacked sample. Sources without a spectroscopic redshift are assigned the mean redshift of the sample to which they belong, where the mean redshifts for the sample are specified in Figure 1.
[e]We only consider BX/BM galaxies which are spectroscopically confirmed to lie at redshifts $z > 1$, $\sim 25\%$ of the photometric sample of BX/BM galaxies.
[f]Photometric BX/BM galaxies.

we may be incomplete for the BzK/PE objects despite the very deep B-band data considered here and these missing objects may be more easily selected using the $J - K_s > 2.3$ criteria discussed below (see also § 4.2.3).

The $J - K_s$ color probes the age-sensitive Balmer and 4000 Å breaks for galaxies with redshifts $2.0 \lesssim z \lesssim 4.5$ (Figure 3). The criterion

$$J - K_s > 2.3 \quad (6)$$

(Franx et al. 2003) can be used to select both passively evolving and heavily reddened star-forming galaxies with $E(B-V) > 0.3$. Galaxies satisfying this criterion are also referred to as Distant Red Galaxies (DRGs; Franx et al. 2003; van Dokkum et al. 2004). There are 62 galaxies with $J - K_s > 2.3$ that are detected in J, and an additional 11 have J-band limits. The observed surface density of DRGs is 1.01 ± 0.12 arcmin^{-2} to $K_s = 21$, in very good agreement with the surface density found by van Dokkum et al. (2004) and Förster Schreiber et al. (2004). The *spectroscopic* redshift distribution of DRGs from the four fields of the optical survey where we have deep J and K_s-band imaging is shown in Figure 1, and is consistent with the redshift distributions found by van Dokkum et al. (2004), van Dokkum et al. (2003), and Förster Schreiber et al. (2004). Star-forming and passively-evolving DRGs are referred to as "DRG/SF" and "DRG/PE", respectively. The depth of our J-band image implies that our sample of DRGs will be incomplete for those with $K_s > 21$. Therefore, we have limited ourselves to galaxies with $K_s < 21$ when comparing DRGs with BzK and/or BX/BM selected galaxies. We reconsider BX/BM and BzK galaxies with $K_s > 21$ as noted below.

The optical magnitude distributions for galaxies with $K_s < 21$ are shown in Figure 4. The catalog of BX/BM galaxies is restricted to $\mathcal{R} < 25.5$. However, our optical imaging is significantly deeper ($\mathcal{R} = 27.5$; 3 σ), allowing us to extract optical magnitudes for galaxies much fainter than those in the BX/BM catalog. Most of those galaxies with $\mathcal{R} > 25.5$ are DRGs. The nature of optically-faint DRGs is discussed in § 4.2.

For most of the analysis that follows, we either use only the spectroscopically confirmed sub-sample of BX/BM galaxies, or we apply our knowledge of the contamination fraction of the photometric sample to deduce any inferred quantities. The small available spectroscopic samples using the near-IR criteria prevent us from applying similar corrections when deducing properties for the near-IR samples.

2.3. *X-ray Data and Stacking Method*

One focus of this paper is to draw comparisons between galaxies selected by the techniques described above by using their stacked X-ray emission as a proxy for their bolometric SFRs. X-ray stacking allows us to determine instantaneous bolometric SFRs in a manner that is independent of extinction and the degeneracies associated with stellar population modeling. For exam-

ple, the average reddening of rest-frame UV selected galaxies of $E(B-V) \sim 0.15$ implies a column density of $N_{\rm H} \sim 7.5 \times 10^{20}$ cm^{-2}, assuming the Galactic calibration (Diplas& Savage 1994). Absorption in the rest-frame $2-10$ keV band is negligible for these column densities. The X-ray data are taken from the *Chandra* 2 Ms survey of the GOODS-N field (Alexander et al. 2003). We made use primarily of the soft band (SB; $0.5-2.0$ keV) data for our analysis, but we also include hard band (HB; $2.0-8.0$ keV) data to examine the nature of directly-detected X-ray sources. The data are corrected for vignetting, exposure time, and instrumental sensitivity in producing the final mosaicked image. The final product has an SB on-axis sensitivity of $\sim 2.5 \times 10^{-17}$ erg s^{-1} cm^{-2} ($3\,\sigma$), sufficient to directly detect $L_{2-10\ \rm keV} > 9.3 \times 10^{41}$ ergs s^{-1} objects at $z \sim 2$, corresponding to an SFR of ~ 190 M$_\odot$ yr^{-1}.

The stacking procedure followed here is the same as that discussed in Reddy & Steidel (2004). Apertures used to extract X-ray fluxes had radii set to $2\farcs5$ for sources within $6'$ of the average *Chandra* pointing origin, and set to the 50% encircled energy radius for sources with off-axis angles greater than $6'$ (Feigelson et al. 2002). X-ray fluxes were computed by adding the counts within apertures randomly dithered by $0\farcs5$ at the galaxy positions. Background estimates were computed by randomly placing the same sized apertures within $5''$ of the galaxy positions, careful to prohibit the placing of a background aperture on a known X-ray detection. This procedure of placing random apertures was repeated 1000 times. The mean X-ray flux of a galaxy is taken to be the average of all the flux measurements from the $0\farcs5$ dithered apertures and the background noise is taken to be the dispersion in fluxes measured from the background apertures. We applied aperture corrections to the fluxes and assumed count rate to flux conversions based on the results compiled in Table 7 of Alexander et al. (2003), a photon index $\Gamma = 2.0$, and a Galactic absorption column density of $N_{\rm H} = 1.6 \times 10^{20}$ cm^{-2} (Stark et al. 1992). Poisson errors dominate the uncertainties in flux.

3. RESULTS

3.1. *Direct X-ray Detections*

Of the 221 BzK/SF candidates with $K_{\rm s} < 21$, 32 (14%) have an X-ray counterpart within $1\farcs5$ (Alexander et al. 2003), with a $\sim 0.22\%$ probability for chance superposition. The X-ray detection fractions are 24%, 6%, and 26%, for the BzK/PE, BX/BM, and DRG samples, respectively, and are summarized in Table 2. Eleven of the 36 directly-detected BzK sources (32 in the BzK/SF sample and 4 in the BzK/PE sample) would not have been detected with the sensitivity of the shallower 1 Msec data in the GOODS-South field studied by Daddi et al. (2004a). After taking into account the sensitivity difference, we find a direct X-ray detection rate comparable to that of Daddi et al. (2004a) of $\sim 11\%$. Figure 5 shows the X-ray/optical flux ratios ($\log f_{\rm X}/f_{\rm R}$) for sources in all four samples (BX/BM, BzK/SF, BzK/PE, and DRG) directly-detected in the *Chandra* hard band ($2-8$ keV). Direct hard band detections must be AGN if they are at $z \sim 2$, since starburst galaxies with no accretion activity are expected to have little flux at rest-frame energies of $6-20$ keV. Indeed, the X-ray/optical flux ratios for directly detected hard band

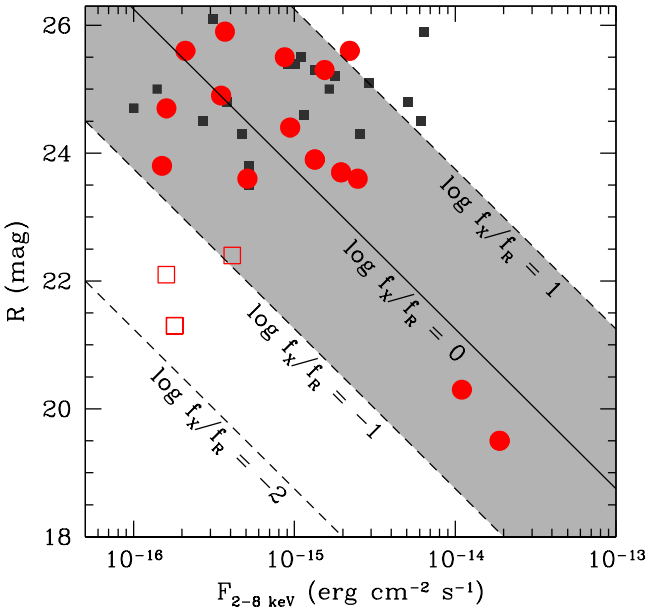

FIG. 5.— Optical/X-ray flux ratios, defined as $\log f_{\rm X}/f_{\rm R} = \log f_{\rm X} + 5.50 + R/2.5$ (Hornschemeier et al. 2001), for all directly detected hard band X-ray sources in the BX/BM, BzK (SF/PE), and DRG samples. The abscissa is the observed hard-band flux, corresponding to rest-frame energies of $6-24$ keV, and the ordinate is the observed *Cousins* R magnitude from the compilation of Barger et al. (2003). Large circles denote sources with spectroscopic redshifts $z > 1$, and are likely AGNs given their direct hard band detections. Sources with hard band detections but no redshift identification are shown by the small squares. Almost all sources have optical/X-ray flux ratios between $-1 < \log f_{\rm X}/f_{\rm R} < 1$ (shaded region), values commonly found for AGNs. Those with $\log f_{\rm X}/f_{\rm R} < -1$ are confirmed interlopers, shown by the large open squares. Starburst galaxies generally have $\log f_{\rm X}/f_{\rm R} < -1$.

sources lie in the region typically populated by AGNs (shaded area of Figure 5). A smaller fraction of galaxies with direct hard band detections (and the three sources with the smallest $\log f_{\rm X}/f_{\rm R}$) are spectroscopically confirmed interlopers at $z < 1$. From Table 2, it is easy to see that much of the AGN contamination in star-forming samples of galaxies (e.g, BX/BM, BzK/SF) occurs for magnitudes $K_{\rm s} < 20$.

Figure 5 only shows those X-ray sources with hard band detections. Eleven additional sources had direct soft band ($0.5-2.0$ keV) detections, but no hard band detections. Of these 11, 5 sources have $R > 22.0$, $f_{0.5-2.0\ \rm keV} \lesssim 0.1 \times 10^{-15}$ erg cm^{-2} s^{-1}, and $\log f_{\rm X}/f_{\rm R} < -1$, indicating they may be starburst galaxies. These 5 sources and their properties are summarized in Table 3. Three of the five sources have spectra taken by us or by Barger et al. (2003) indicating no obvious AGN spectral features. These sources may be rapidly star-forming galaxies and for fairness we include them in the stacking analysis as indicated below and in Table 2.

It is interesting to also consider the rest-frame near-IR properties of the directly detected X-ray sources as indicated by their *Spitzer*/IRAC colors. Figure 6 shows the $3.6-5.8$ μm color as a function of 3.6 μm magnitude for all samples considered here. There is a clear segregation in the IRAC colors of X-ray detections where they show, on average, brighter IRAC magnitudes and redder IRAC colors when compared with the colors of star-forming galaxies in the BX/BM and BzK/SF sam-

TABLE 3. POSSIBLE STAR-FORMING DIRECT X-RAY DETECTIONS

α (J2000.0)	δ (J2000.0)	Sample	z	$f_{0.5-2.0\ \mathrm{keV}}$[a] ($\times 10^{-15}$ erg s^{-1} cm^{-2})	K_s (Vega mag)	R[a] (mag)	log f_X/f_R[b]
12:36:21.95	62:14:15.5	BzK/SF	1.38	0.02	18.95	23.1	-1.96
12:36:52.75	62:13:54.8	BX/BM	1.36	0.03	19.54	22.1	-2.18
12:36:53.46	62:11:40.0	BX/BM;BzK/SF	...	0.11	18.65	22.7	-1.38
12:36:56.89	62:11:12.1	BzK/SF	...	0.02	20.50	23.8	-1.68
12:37:03.70	62:11:22.6	BX/BM;BzK/SF	1.72	0.04	19.92	23.4	-1.54

[a]Soft-band fluxes are from Alexander et al. (2003) and *Cousins* R magnitudes are from Barger et al. (2003).
[b]Defined as $\log f_X/f_R = \log f_X + 5.50 + R/2.5$ (Hornschemeier et al. 2001).

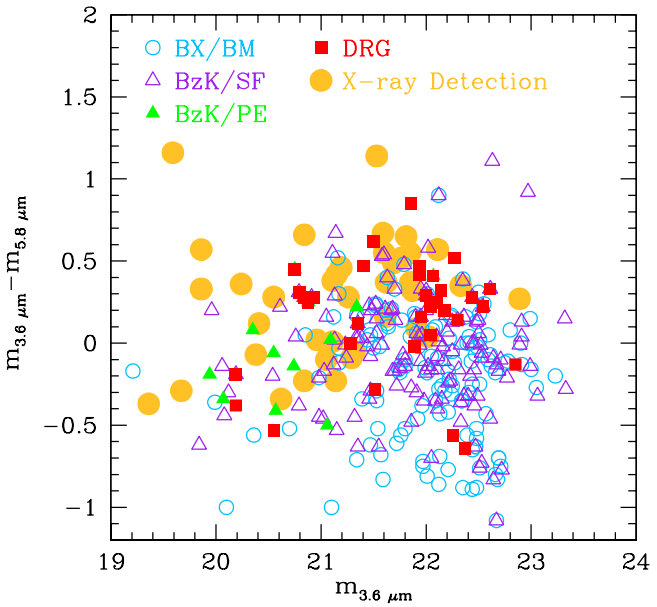

FIG. 6.— *Spitzer*/IRAC $3.6-5.8$ μm color versus 3.6 μm magnitude (in AB units) for all samples considered here, with emphasis on directly detected X-ray sources (large circles). These direct detections generally have brighter IRAC magnitudes and redder colors than star forming BX/BM and BzK/SF galaxies, likely due to thermal continuum from circumnuclear dust proximate to the AGN.

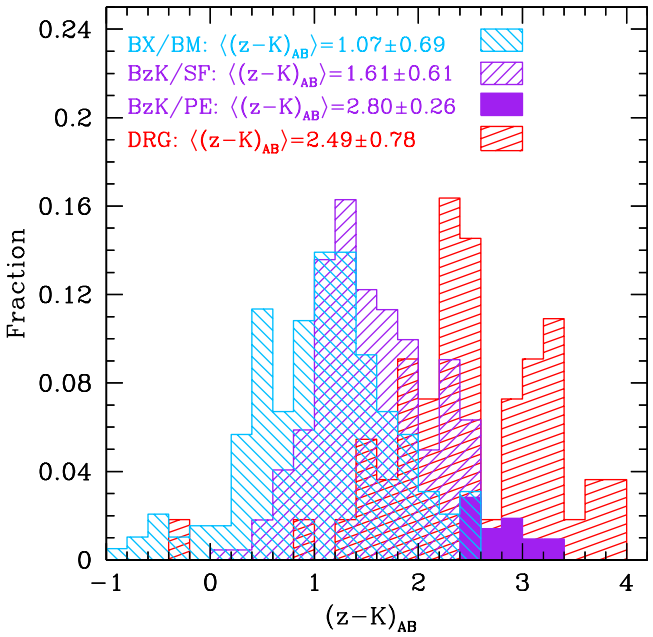

FIG. 7.— $z-K$ color distribution for BX/BM, star-forming BzK, and DRG galaxies to $K_s = 21$. The mean $z-K$ color of galaxies becomes redder for the BX/BM to BzK to DRG samples. BX/BM selection is more efficient in selecting objects with blue $(z-K)_{AB} \lesssim 1$ and DRG selection is more efficient in selecting objects with very red $(z-K)_{AB} \gtrsim 3$. The BzK criteria spans the middle range of $(z-K)_{AB}$ color. The small solid histogram shows the arbitrarily normalized distribution in $(z-K)_{AB}$ color for passively-evolving BzK galaxies.

ples. Such a trend might be expected if the rest-frame near-IR light from the X-ray sources is dominated by thermal continuum from circumnuclear dust heated by the AGN. The increase in flux density across the IRAC bands for AGN has been seen for ERO samples at redshifts $z \sim 1-3$ (Frayer et al. 2004), similar to what is observed here. Finally, the 5 objects listed in Table 3 have $m_{3.6\mu m-5.8\mu m} \sim -0.35$ to 0.35 and $m_{3.6\mu m} = 20.2-22.0$, lying in the same region of IRAC color space as some of the star-forming BX/BM and BzK/SF candidates.

At times in the following analysis, we also consider submillimeter galaxies and their relation to optical and near-IR selected objects. These heavily star-forming objects are generally associated with directly-detected X-ray sources, and we reconsider the X-ray emission from these sources as pointed out below. Unless otherwise stated, however, we have excluded all directly-detected hard band X-ray sources from the analysis under the assumption that their X-ray emission is contaminated by AGN.

3.2. *Overlap Between Samples*

Galaxies selected solely by the presence of some unobscured star-formation (BX/BM selection), and those selected by some combination of stellar mass and star-formation (DRG and BzK selection) can be distinguished by their observed near-IR color distributions (Figure 7). The mean $(z-K)_{AB}$ color for BX/BM galaxies is ~ 0.54 mag bluer than the BzK/SF sample, just within the 1 σ dispersion of both samples. This difference in average $(z-K)_{AB}$ color between BX/BM and BzK/SF galaxies partly stems from the fact that the width of the BzK selection window below $(z-K)_{AB} = 1$ narrows to the point where photometric scatter becomes increasingly important in determining whether a galaxy with blue colors (i.e., $(z-K)_{AB} < 1$) is selectable with

the BzK/SF criteria[4]. On the other hand, the BX/BM criteria are less efficient than BzK selection for galaxies with $(z-K)_{\rm AB} \gtrsim 1.6$. BX/BM galaxies with red near-IR colors are systematically fainter in the optical than those with blue near-IR colors (Figure 8), reflecting both the correlation between $\mathcal{R}$ and z as these filters lie close in wavelength, as well as the $K_{\rm s} < 21$ limit adopted in Figure 8. Therefore, the optical catalog limit of $\mathcal{R} = 25.5$ would appear to exclude from the BX/BM sample those galaxies with $(z-K)_{\rm AB} \gtrsim 3$ (Figure 8). As we show § 4, the exclusion of $(z-K)_{\rm AB} \gtrsim 3$ galaxies by optical selection is not a fault of the criteria themselves: the $\mathcal{R} = 25.5$ limit is imposed so that spectroscopic followup is feasible on the candidate galaxies. Rather, the exclusion of $(z-K)_{\rm AB} \gtrsim 3$ galaxies from optical surveys simply reflects a fundamental change in the star formation properties of such red galaxies.

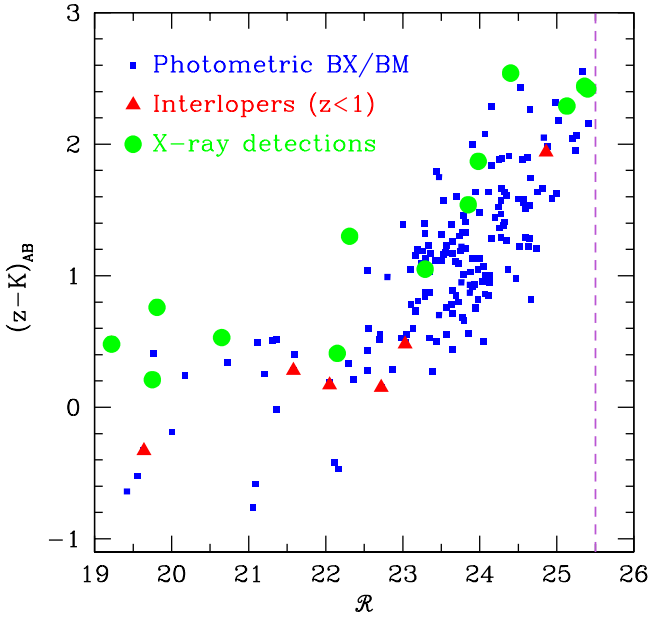

FIG. 8.— $(z-K)_{\rm AB}$ versus $\mathcal{R}$ for photometric BX/BM galaxies (squares) to $K_{\rm s} = 21$, showing that optically selected galaxies with red near-IR colors are optically fainter on average than those with blue near-IR colors. This effect is due to the $K_{\rm s} = 21$ limit as well as the correlation between $\mathcal{R}$ and z-band magnitude as the two filters lie close in wavelength. Objects with $(z-K)_{\rm AB} \gtrsim 2.6$ are missed by BX/BM selection as they fall below the $\mathcal{R} = 25.5$ BX/BM catalog limit (dashed vertical line). Also shown are BX/BM sources with direct X-ray detections (large circles) and spectroscopically confirmed interlopers (triangles).

Separately, DRGs have a very red $\langle (z-K)_{\rm AB} \rangle = 2.49 \pm 0.78$. Approximately 10% of $z > 1.4$ BzK/SF galaxies also have $J - K_{\rm s} > 2.3$ (Figure 9), similar to that found by Daddi et al. (2004a). The fact that there is some, albeit small, overlap between the BzK/SF and DRG samples is not surprising since the two criteria can be used to target reddened galaxies and both have redshift distributions that overlap in the range $2.0 < z < 2.6$ (Figure 1). The DRG fraction among BzK selected galaxies does not change appreciably if we add in the

[4] None of the selection criteria considered here have boxcar selection functions in either color or redshift space due to various effects, including photometric errors. The effect of this is to suppress the efficiency for selecting objects whose intrinsic colors lie close to the edges of the selection window.

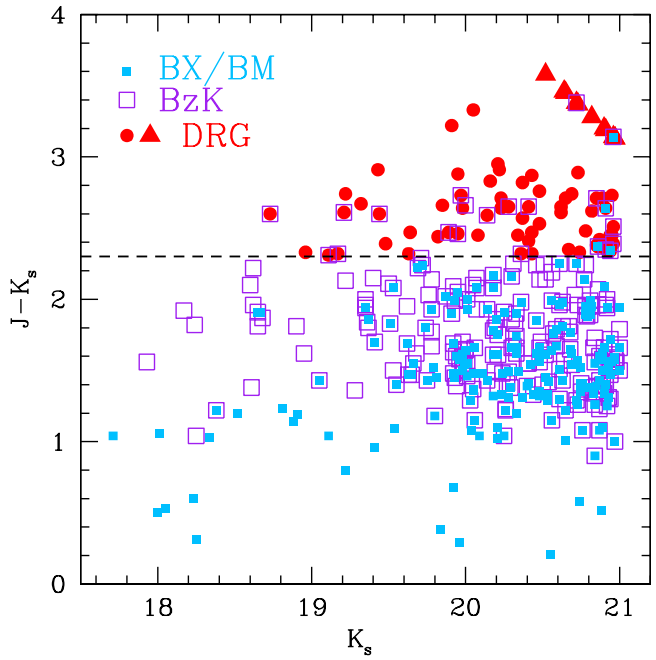

FIG. 9.— $J - K_{\rm s}$ color versus $K_{\rm s}$ for BX/BM (filled squares), BzK (open squares), and DRG (circles) samples to $K_{\rm s} = 21$. The hashed horizontal line denotes the $J - K_{\rm s} = 2.3$ limit. DRGs with limits in J-band are indicated by the triangles. Approximately 5% of DRGs satisfy the BX/BM criteria, but the fraction rises to $\sim 12\%$ if we include those selected by the $z \sim 3$ LBG criteria.

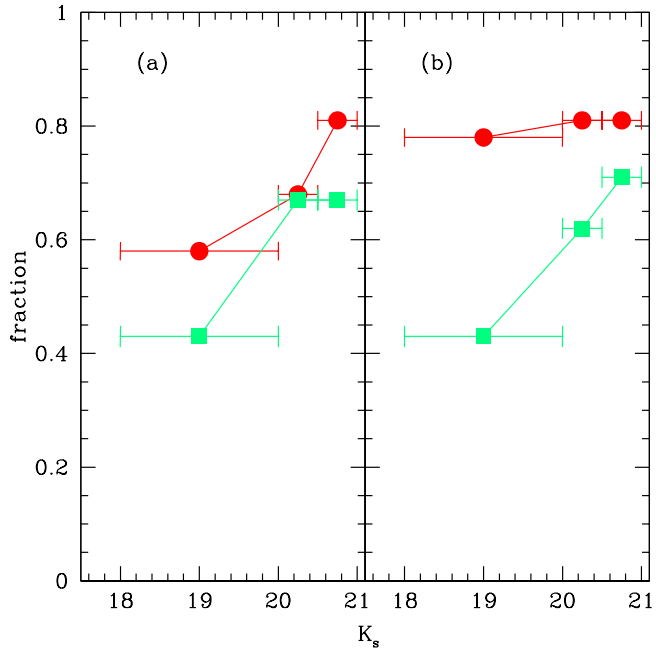

FIG. 10.— (a) Fraction of BzK/SF sources which are optically selected with the BX/BM criteria when including (squares) and excluding (circles) directly detected X-ray sources that are likely AGN (§ 3.1); (b) Fraction of photometric BXs and BMs that are BzK/SF selected (squares) and the fraction of BXs and BMs with confirmed redshifts $z > 1.4$ that are BzK/SF selected (circles).

BzK/PE sources—only 5 of 17 BzK/PE galaxies have $J-K_{\rm s} > 2.3$—as the BzK/PE galaxies are mostly at redshifts lower than the DRGs ($z \lesssim 2$). Finally, we note that DRGs include objects with much redder $(z-K)_{\rm AB}$ colors

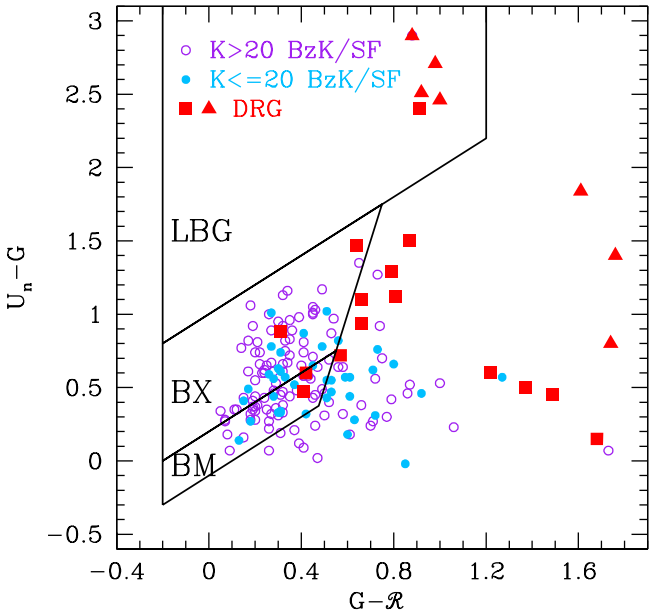

FIG. 11.— BX/BM colors of BzK/SF galaxies (circles) and DRGs with $\mathcal{R} < 25.5$, excluding direct X-ray detections. Squares denote DRGs with $> 5\ \sigma$ detections in U_n, G, and $\mathcal{R}$; triangles denote DRGs with $5\ \sigma$ limits in U_n. All points are for galaxies with $K_s < 21$. Also indicated are the BX/BM selection criteria for $z \sim 2$ BMs and BXs, as well as the $z \sim 3$ LBG criteria of Steidel et al. (2003). Approximately 40% of our DRG sample galaxies have $\mathcal{R} < 25.5$. Of all DRGs, including those not shown in the figure and which have $\mathcal{R} > 25.5$, $\sim 12\%$ can be selected using the BX, BM, or LBG criteria. Note the number of BzK and DRG galaxies that lie very close (e.g., within $\lesssim 0.2$ mag) of the BX/BM selection windows.

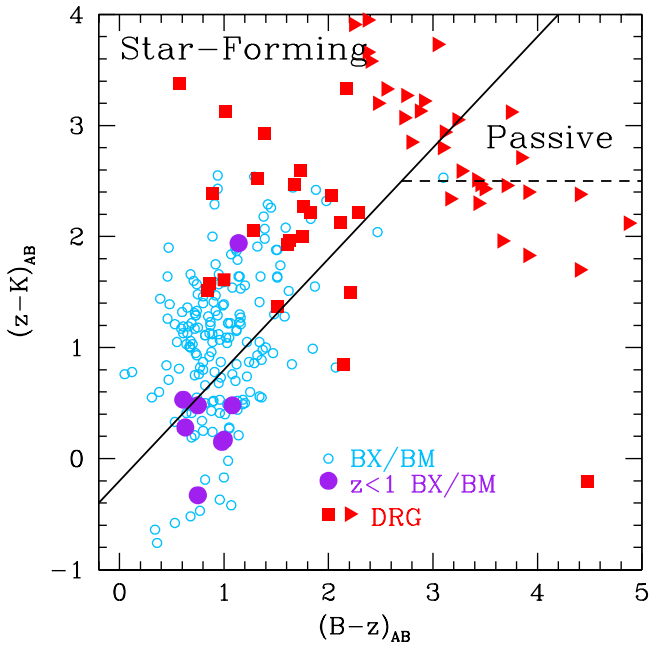

FIG. 12.— BzK colors of BX/BM galaxies (empty circles) and DRGs (filled squares) to $K_s = 21$. Large filled circles denote BX/BM objects with spectroscopically confirmed redshifts $z < 1$ (interlopers), most of which fall outside the BzK/SF selection window. Also shown is the expected region of color space for passively evolving $z > 1.4$ galaxies (Daddi et al. 2004a). Note the number of BX/BM galaxies that lie very close (e.g., within $\lesssim 0.2$ mag) of the BzK selection window. DRGs with B-band limits, shown by the triangles, cluster in the region expected for passively evolving $z > 1.4$ galaxies.

than found among BX/BM and BzK/SF/PE galaxies, i.e. those with $(z - K)_{AB} > 3$. The absence of these galaxies from star-forming selected samples is discussed in § 4.2.

We can directly quantify the overlap between BzK/SF and BX/BM galaxies. Figure 10 shows the fraction of BzK/SF galaxies satisfying the BX/BM criteria (left panel) and the fraction of BX/BM galaxies satisfying the BzK/SF criteria (right panel). Most of the contamination of the BzK/SF sample (that we know of) is from X-ray detected AGN (§ 3.1), while most of the contamination of the BX/BM sample is from low redshift interlopers (Table 1). Both sources of contamination tend to occupy the bright end of the K-band apparent magnitude distribution. We also show the overlap fractions in Figure 10 excluding X-ray detected AGN and interlopers. The BX/BM criteria recover an increasing fraction of BzK/SF selected sources proceeding from $K_s < 20$ galaxies ($\sim 60\%$ recovery fraction) to $K_s \sim 21$ galaxies ($\sim 80\%$ recovery fraction) after excluding directly detected X-ray sources which are likely AGN (see § 3.1). Conversely, the BzK/SF criteria recover $\sim 80\%$ of spectroscopically confirmed BX/BM galaxies at $z > 1.4$, and are evidently effective at recognizing most of the BX/BM low redshift interlopers that tend to occupy the bright end of the K-band apparent magnitude distribution. This result stems from the fact that low redshift interlopers tend to have bluer colors than necessary to satisfy the BzK/SF criteria.

Figures 11 and 12 show that a significant portion of BzK/SF galaxies missed by BX/BM selection, and conversely, have colors that place them within $\lesssim 0.2$ mag of the selection windows, which is comparable to the photometric uncertainties. The BX/BM criteria likely miss some BzK/SF galaxies not because of some failure of the criteria, but because we cannot measure photometry with infinite precision. The trend from lower (60%) to higher (80%) recovery rate shown in Figure 10a reflects the fact that a greater percentage of $K_s < 20$ BzK/SF galaxies have redder $G - \mathcal{R}$ colors (when compared with $K_s > 20$ BzK/SF galaxies) than required to satisfy the BX/BM criteria (Figure 11). There are some BzK/SF galaxies which have very red $G - \mathcal{R} \gtrsim 0.8$ colors. As we show in § 4, these red $G - \mathcal{R}$ galaxies would have an average bolometric SFR similar to BzK/SF galaxies with bluer $G - \mathcal{R}$ colors if they are at similar redshifts, $z \sim 2$. Therefore, if these red objects are at $z \sim 2$, then the correlation between $G - \mathcal{R}$ and reddening, as quantified by the Calzetti et al. (2000) law, would appear to fail. Photometric scatter will also reduce the effectiveness of the BzK criteria in selecting BX/BM galaxies (Figure 12). We can account for most of the photometric incompleteness using the more sophisticated analysis of Reddy et al. (2005).

Our deep K-band data allow us to investigate the efficiency of BzK/SF selection to fainter K magnitudes than previously possible. Figure 13 shows the BzK colors of BX/BM galaxies with spectroscopic redshifts $1.4 < z < 2.6$ for three bins in K_s magnitude. The BzK/SF criteria were designed to select relatively massive galaxies with $K_s < 20$, but they become slightly

less efficient in culling $K_s > 21$ galaxies: 10 of 49 ($\sim$ 20%) BX/BM galaxies with spectroscopic redshifts $1.4 < z < 2.6$ and $K_s > 21$ do not satisfy the BzK/SF criteria. Furthermore, we note that $\sim$ 11% (61/544) of BX/BM candidates that fall in the region with K-band data are undetected to $K_s = 22.5$ (3 σ). The K-band limits for these galaxies suggests they are younger star-forming systems with $(z-K)_{AB} \lesssim 1$, below which the BzK/SF criteria drop in efficiency, as discussed above. We remind the reader that many of the BzK/SF objects not appearing in the BX/BM sample may be missed by the BX/BM criteria simply because of photometric errors. BX/BM galaxies missed by the BzK/SF criteria may be missed not because of intrinsic differences in the objects, but simply because of photometric scatter or because of the difficulty in obtaining very deep K_s-band data.

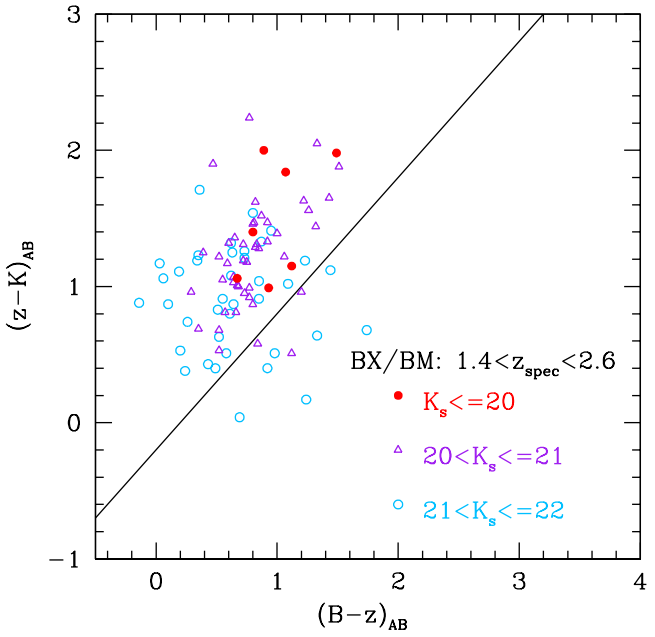

FIG. 13.— BzK colors of spectroscopically confirmed BX/BM galaxies with redshifts $1.4 < z < 2.6$ for different bins in K_s magnitude. BzK/SF selection appears to miss an increasing fraction of $K_s > 21$ galaxies in this redshift range due to the narrowing BzK/SF selection window for objects with bluer $(z-K)_{AB}$ colors. In addition, $\sim$ 19% of BX/BM candidates have $K_s > 22.0$ and are not shown.

Turning to $J - K_s > 2.3$ galaxies, we show the optical colors of DRGs with $\mathcal{R} < 25.5$ in Figure 11, and the near-IR colors of the 74% of DRGs with z-band detections in Figure 12. The optical criteria are particularly inefficient in selecting $J-K_s > 2.3$ sources: 9 of 73 (12%) of DRGs in the GOODS-N field satisfy BX, BM, or LBG selection. This fraction is similar to the overall detection rate found by Erb et al. (2005) for the 4 fields in the $z \sim 2$ optical survey with deep J and K-band data. The LBG criteria can be used to select some DRGs since $z \sim 2$ galaxies with a Calzetti reddened constant star formation SED with $E(B-V) \gtrsim 0.3$ are expected to lie in the color space occupied by $z \sim 3$ LBGs. A greater fraction ($\sim$ 30%) of DRGs satisfy the BzK/SF criteria (Figure 12) since these criteria select objects with developed spectral breaks and with redshifts that fall in the range probed by DRG selection (see Figure 1). We note that DRGs with B-band limits cluster in the region of color space expected for passively evolving $z > 1.4$ galaxies (Figure 12). These DRGs have little, if any, current star formation (see § 4.2).

3.3. *Stacked X-ray Results*

The X-ray data are not sufficiently sensitive to detect individual galaxies with SFR$\lesssim$ 190 $M_\odot$ yr^{-1} (3 σ). We can, however, stack the X-ray data for subsets of galaxies below the sensitivity threshold to determine their average X-ray emission. The influence of AGN in any X-ray stacking analysis is a concern. The softness of a stacked signal provides some circumstantial evidence for X-ray emission due primarily to star formation (e.g., van Dokkum et al. 2004, Daddi et al. 2004a, Laird et al. 2005). UV line signatures and radio emission can provide additional constraints on the presence of AGN (e.g., Reddy & Steidel 2004). We typically removed all directly-detected X-ray sources from the optical and near-IR samples before running the stacking simulations, except as noted below and in Table 3 when considering X-ray detected sources which may be star-forming galaxies. Our method of excluding other X-ray detected sources ensures that luminous AGN do not contaminate the stacked signal. Indirect evidence suggests that less luminous AGN do not contribute significantly to the stacked signal. First, the stacked signal has no hard band (HB; $2-8$ keV) detection indicating that the signal is softer than one would expect with a significant AGN contribution. Second, the availability of rest-frame UV spectra for many of the BX/BM objects provides an independent means of identifying AGN. There is one source whose spectrum shows high-ionization emission lines in the rest-frame UV, but no X-ray detection in the *Chandra* 2 Ms data. Removing this X-ray faint AGN source does not appreciably affect the stacked X-ray flux. In addition, Reddy & Steidel (2004) examined the very same BX/BM dataset used here and found a very good agreement between dust-corrected UV, radio, and X-ray inferred SFRs for the sample, suggesting star formation as the dominant mechanism in producing the observed multi-wavelength emission. Finally, the local hosts of low luminosity AGN have stellar populations characteristic of passively evolving early-type galaxies (Kauffmann et al. 2003). In § 4.2 we show that passively evolving galaxies at $z \sim 2$ have little or no detectable X-ray emission, implying that low level accretion activity in these systems does little to alter the X-ray emission relative to that produced from star formation. The absence of X-ray emission from these passively evolving galaxies also suggests that low mass X-ray binaries contribute little X-ray emission in star-forming galaxies when compared with the emission produced from more direct tracers of the current star formation rate, such as high mass X-ray binaries.

Stacking results for the samples (to $K_s = 22.5$) are summarized in Figure 14 and Table 2. The left panel of Figure 14 includes all photometrically-selected BzK/SF and DRG galaxies, and all spectroscopically-confirmed $z > 1$ BX/BM galaxies. The right panel includes only those BzK/SF galaxies with spectroscopic redshifts $z > 1$, all of which also satisfy the BX/BM criteria. All direct X-ray detections have been excluded in making Figure 14. The distributions do not change appreciably

if we only consider the X-ray flux of BzK/SF galaxies spectroscopically confirmed to lie at $z > 1$ (Figure 14b). Removing the one spectroscopic $z > 1$ AGN undetected in X-rays does little to change the X-ray luminosity distributions. The luminosity distributions agree well between the three samples over a large range in K_s magnitude, with $K_s < 20$ galaxies exhibiting the largest X-ray luminosities by a factor of two to three when compared with fainter $K_s > 20.5$ galaxies.

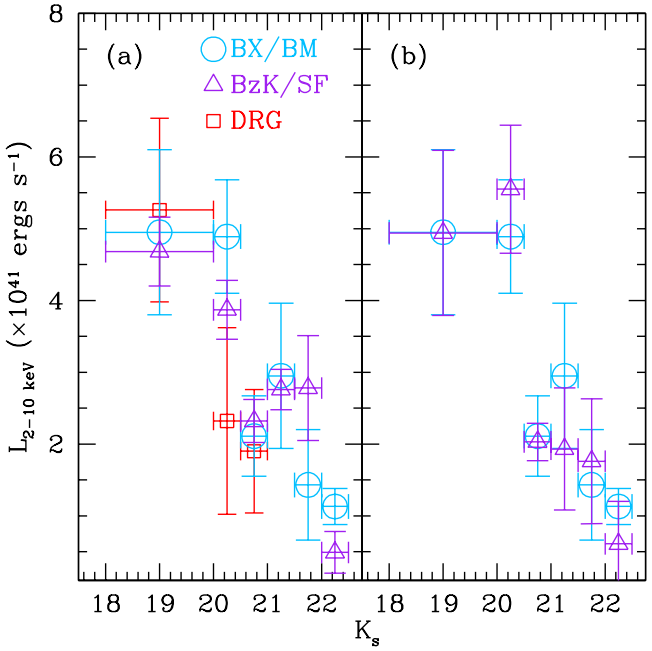

FIG. 14.— Stacked X-ray luminosity versus K_s magnitude for BX/BM galaxies with $z > 1$ (circles), BzK/SF galaxies (triangles), and DRGs (squares), excluding all directly detected X-ray sources. The left and right panels show the distributions for photometric and spectroscopically confirmed $z > 1$ BzK/SF galaxies, respectively. Sources without a spectroscopic redshift were assigned the mean redshift of the sample which they belong to, according to Figure 1. In all cases, we find the distributions consistent within the errors. We also find that $K_s < 20$ galaxies have average X-ray luminosities that are a factor of $2-3$ times higher than that of $K_s > 20.5$ galaxies.

4. DISCUSSION

In this section we first present the X-ray inferred average bolometric SFRs for galaxies in the BX/BM, BzK/SF/PE, and DRG samples, and compare our results with other X-ray stacking analyses. Unless stated otherwise, we exclude hard band X-ray AGN sources from the analysis of the SFRs. The SFRs are interpreted for galaxies as a function of their near-IR colors and we assess the ability of optical surveys to single out both heavily reddened and massive galaxies. We identify passively evolving galaxies at $z \sim 2$ from their red near-IR colors and discuss plausible star formation histories for these galaxies using the X-ray data as an additional constraint. Finally, we discuss the contribution of BX/BM, BzK/SF, and DRG galaxies to the star formation rate density at $z \sim 2$, taking into account the overlap between the samples and their respective redshift distributions.

4.1. *Star Formation Rate Distributions*

Star Formation Rates and Comparison with Other Studies

We estimated the SFRs for galaxies in our samples using the Ranalli et al. (2003) calibration between X-ray and FIR luminosity. This calibration reproduced the SFRs based on independent star formation tracers for $z \sim 2$ galaxies (Reddy & Steidel 2004), so we are confident in using it here. The SFR distributions for BX/BM, BzK, and DRG galaxies are shown in Figure 15, where we have added the 5 directly-detected soft band X-ray sources in Table 3 that may be star-forming galaxies. The SFRs are summarized in Table 2. The mean SFR of $K_s < 20$ galaxies is $\sim 90 - 140$ M$_\odot$ yr^{-1}, and is a factor of $2-3$ times larger than galaxies with $K_s > 20.5$. For comparison, Daddi et al. (2004a) found an average SFR of K20 galaxies in the GOODS-South field of 190 M$_\odot$ yr^{-1} (including one likely star-forming galaxy directly detected in X-rays). This is somewhat higher than our value of 110 M$_\odot$ yr^{-1} for $K_s < 20$ BzK/SF galaxies. This discrepancy could simply result from field-to-field variations, small number statistics, or the lower sensitivity of the X-ray data in the GOODS-South field compared to GOODS-North. With the *Chandra* 2 Ms data, we are able to exclude directly-detected X-ray sources down to a factor of two lower threshold than was possible with the 1 Ms data in the GOODS-South field. If we add back those $K_s < 20$ X-ray BzK/SF galaxies that would have been undetected in the 1 Ms data to the stacking analysis, we obtain an average SFR of 160 M$_\odot$ yr^{-1}, more in line with the Daddi et al. (2004a) value of 190 M$_\odot$ yr^{-1}.

A similar stacking analysis by Rubin et al. (2004) indicates that $K_s < 22$ DRGs have SFRs of ~ 280 M$_\odot$ yr^{-1}, corrected for the difference in SFR calibration used here and in Rubin et al. (2004). This very high value is likely a result of the shallow X-ray data (74 ksec) considered in that study; the depth of their X-ray data precludes the removal of most of the X-ray sources that are directly detected in the 2 Ms X-ray survey. If we include those X-ray sources that would have been undetected in the 74 ksec data, assuming a mean redshift of $\langle z \rangle = 2.4$, the average SFR for the DRGs with $K_s < 21$ is 250 M$_\odot$ yr^{-1}. Therefore, much of the difference in the SFRs can be attributed to unidentified AGN in the shallower X-ray surveys contaminating estimates of the star formation rate. If Figure 15 is any indication, then adding DRGs with $21 < K_s \leq 22$ to the stack would decrease this average SFR. Variance of the fraction of DRG/PE galaxies between fields may also affect the average SFRs: a greater fraction of DRG/PEs in the GOODS-N field, $\sim 25\%$ (3/13) of which have $K_s < 20$, will lead to a lower *average* SFR for $K_s < 20$ DRGs. As we show in § 4.4.2, there are clearly some number of very reddened galaxies with large SFRs (e.g., submillimeter galaxies) among DRGs (and among the BX/BM and BzK/SF samples). Regardless, these calculations underscore the importance of factoring in the differing sensitivity limits of the various X-ray surveys before comparing results. The strong dependence of SFR with K_s magnitude (Figure 15) also suggests that fair comparisons of the SFRs of galaxies selected in different surveys can only be made between objects with similar rest-frame optical luminosities.

Our analysis is advantageous as we are able to compare

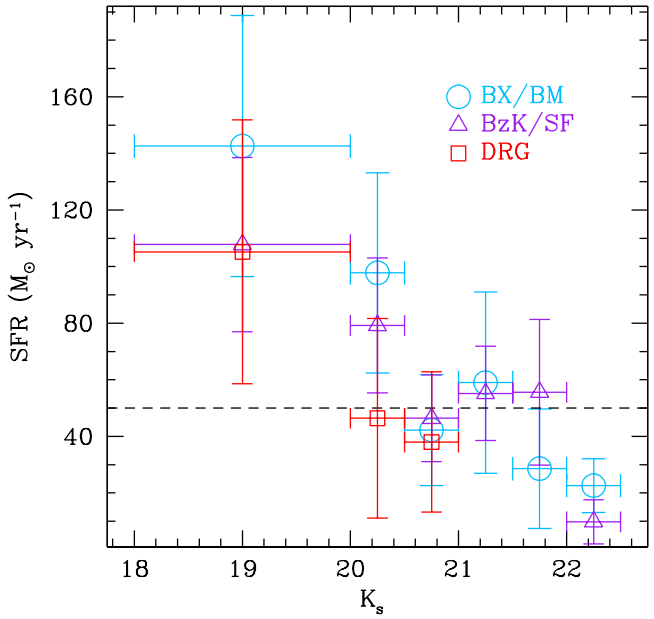

FIG. 15.— Star formation rates inferred from the X-ray luminosity using the Ranalli et al. (2003) calibration. We have added the 5 directly-detected soft band X-ray sources that may be star-forming (Table 3) to compute the average SFR. Circles, triangles and squares denote BX/BM, BzK, and DRG samples, respectively. The BX/BM points are for spectroscopically confirmed $z > 1$ galaxies, and we have assumed the mean redshifts for the BzK/SF and DRG samples as in Figure 14. Uncertainties in the star formation rates are dominated by scatter in the X-ray/FIR relation and the dispersion in the stacked X-ray estimates. The dashed horizontal line denotes the average SFR for the entire spectroscopic ($z > 1$) BX/BM sample of ~ 50 M$_\odot$ yr^{-1} from Reddy & Steidel (2004). Galaxies with $K_s < 20$ have inferred star formation rates a factor of $2-3$ higher than for $K_s > 20.5$ galaxies.

the SFRs of galaxies within the same field, employing the same multi-wavelength data (to the same sensitivity level) and the same photometric measurement techniques, for a consistent comparison. The inferred average SFRs of BzK/SF and DRG galaxies are remarkably similar to that of optically selected galaxies once the samples are restricted to similar K_s magnitudes. The previously noted discrepancies in X-ray inferred SFRs of BzK/SF, DRG, and BX/BM galaxies are therefore likely a result of a mismatch between X-ray survey limits and near-IR magnitude ranges. Field-to-field variations may also partly account for the previously observed discrepancies.

Dependence of SFR on $(z-K)_{AB}$ Color

We began our analysis by noting the differences between the $(z-K)_{AB}$ color distributions of optical and near-IR selected galaxies (Figure 7). Figure 15 indicates that despite these near-IR color differences, the BX/BM, BzK, and DRG galaxies have very similar *average* SFR distributions as a function of K_s magnitude. Another proxy for stellar mass is the $(z-K)_{AB}$ or $\mathcal{R}-K_s$ color (e.g., Shapley et al. 2005) as it directly probes the strength of the Balmer and 4000 Å breaks. Figure 16 shows the inferred average SFRs of optical and near-IR selected galaxies as a function of their $(z-K)_{AB}$ color, excluding all directly-detected X-ray sources[5]. Within any single sample, objects with red $(z-K)_{AB}$ colors up to $(z-K)_{AB} \sim 3$ have the largest SFRs. The red $(z-K)_{AB}$ color for these objects with high SFRs likely results from a developed spectral break (due to an older stellar population) combined with the effects of dust. In fact, Figure 17 illustrates the tendency for BX/BM objects with spectroscopic redshifts $z > 1$ and red $(z-K)_{AB}$ colors to have larger attenuation, as parameterized by $E(B-V)$, on average, than those with bluer $(z-K)_{AB}$ colors. The turnover in the inferred SFR around $(z-K)_{AB} \sim 3$ is discussed in the next section.

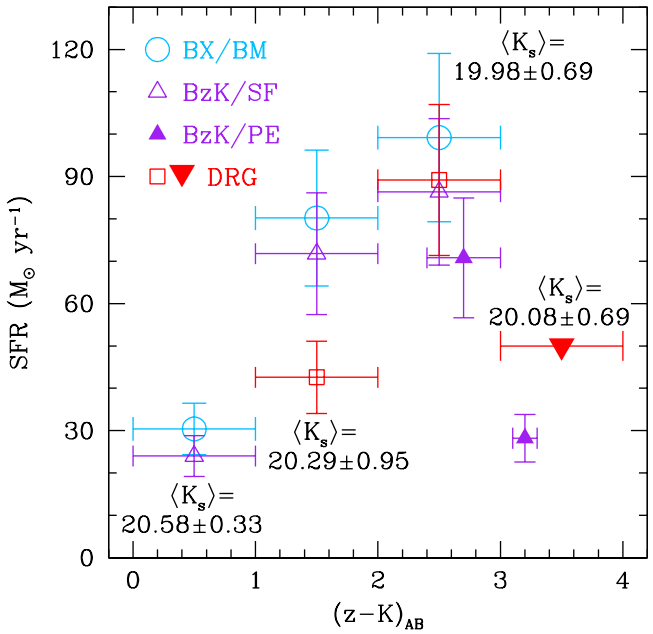

FIG. 16.— Star formation rates of $K_s < 21$ galaxies as a function of $(z-K)_{AB}$ color. Symbols are the same as in Figure 15. The small solid triangles denote the average SFR inferred for BzK galaxies that are selected to be passively evolving (BzK/PE galaxies) and the large inverted triangle indicates the limit in SFR found for the 13 DRGs with $(z-K)_{AB} > 3.0$. Note the turnover in inferred SFR at $(z-K)_{AB} \sim 3$. Also indicated are the average K_s magnitudes for sources in each bin of $(z-K)_{AB}$ color.

Figure 16 suggests that optically selected BX/BM galaxies may have systematically higher SFRs than BzK and DRG galaxies with similar $(z-K)_{AB}$ colors, perhaps indicating that the stacked sample for BzK/SF and DRG galaxies includes those which are passively evolving. This may be particularly true of DRGs, quite a few of which only have B-band limits and which cluster in the BzK color space occupied by passively evolving galaxies (Figure 12). We can assess the dispersion in SFRs by separately stacking galaxies that are expected to be currently star-forming based on their colors and those that are not. For example, the average SFR computed for BzK/SF galaxies that are *not* selected by the BX/BM criteria (of which $\sim 70\%$ are within 0.2 mag of the BX/BM selection windows) is ~ 70 M$_\odot$ yr^{-1}, comparable to the average SFR of all BzK/SF galaxies with $K_s < 21$. *In summary, star-forming BzK galaxies have similar SFRs regardless of whether or not they satisfy the* BX/BM *criteria.* The BX/BM criteria miss some BzK/SF galaxies either because of photometric scatter or because their optical colors are not indicative of their reddening. It is worth noting that photometric scatter

[5] Adding the 5 sources in Table 3 does not appreciably affect Figure 16

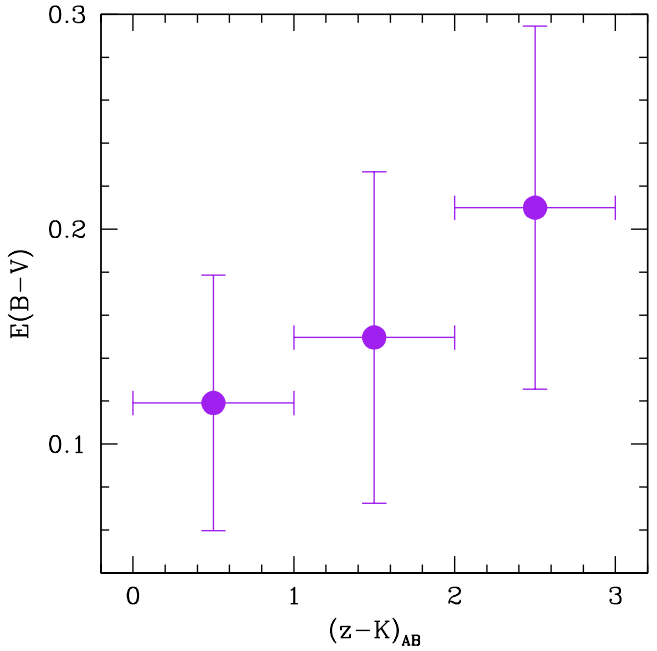

FIG. 17.— Attenuation, as parameterized by the rest-frame UV spectral slope, $E(B-V)$, as a function of $(z-K)_{\rm AB}$ color for spectroscopically confirmed BX/BM galaxies with $z > 1$. Errors in $E(B-V)$ represent the 1 σ dispersion of $E(B-V)$ values for each bin of $(z-K)_{\rm AB}$.

works both ways: some sources with intrinsic colors satisfying the BX/BM criteria will be scattered *out* of the BX/BM selection windows and some whose colors do not satisfy the BX/BM criteria will be scattered *into* the BX/BM selection windows, although the two effects may not equilibrate (Reddy et al. 2005). The incompleteness of the BX/BM and BzK/SF criteria with respect to all star-forming galaxies at $z \sim 2$ simply reflects our inability to establish perfect selection criteria immune to the effects of photometric scatter and SED variations while at the same time efficiently excluding interlopers (e.g., Adelberger et al. 2004). However, the advantage of *spectroscopic* optical surveys is that their selection functions can be quantified relatively easily (e.g., Adelberger et al. 2004, Reddy et al. 2005).

Optical Selection of Reddened Star-Forming Galaxies

Naively, one might interpret the inferred SFRs as a function of $(z-K)_{\rm AB}$ color combined with the results shown in Figure 8 to suggest that BX/BM selection may miss the most actively star-forming galaxies at $z \sim 2$. We can interpret the similarity in SFRs of BX/BM and BzK/SF galaxies in the context of their reddening, as parameterized by their rest-frame UV spectral slopes, $E(B-V)$. Daddi et al. (2004a) show that the reddening vector is essentially parallel to the BzK limit defined by Equation 4, implying that BzK selection should be sensitive to galaxies with higher extinction (and presumably higher star formation rates) than found among BX/BM selected galaxies (i.e., $E(B-V) \geq 0.3$). However, the similarity in the average SFRs of BX/BM and BzK/SF galaxies suggests several possibilities. First, we noted above that BzK/SF galaxies not selected by the BX/BM criteria have similar SFRs as those which do satisfy the BX/BM criteria[6]. Consequently, BzK/SF galaxies with large SFRs that do not satisfy the BX/BM criteria because they truly have $E(B-V) > 0.3$ may not exist in sufficient numbers to significantly change the *average* SFRs for all BzK/SF galaxies which do not satisfy the BX/BM criteria. Adelberger & Steidel (2000) and Laird et al. (2005) find that optically selected galaxies with $z \gtrsim 1$ show no correlation between their rest-frame UV luminosities and their obscuration, implying that on average the redder (more obscured) galaxies have higher bolometric SFRs than galaxies with less reddening. Therefore, the similarity in the average X-ray inferred SFRs of BX/BM and BzK/SF galaxies suggests that there are not large numbers of galaxies with $E(B-V) \gtrsim 0.4$ (i.e., if there were a large number of such heavily reddened objects, their bolometric SFRs would imply X-ray luminosities large enough to be directly detected in the soft band X-ray data, and very few likely star-forming galaxies at these redshifts are directly detected in the soft band).

Second, studies of the UV emission from submillimeter galaxies (SMGs) suggest that heavily reddened galaxies may have similar rest-frame UV spectral properties, such as their range in $E(B-V)$, as those which are forming stars at modest rates, implying that the correlation between $E(B-V)$ and bolometric SFR (e.g., from the Meurer et al. 1999 and Calzetti et al. 2000 laws) breaks down for the most actively star-forming galaxies (e.g., Chapman et al. 2005). Table 4 summarizes the properties of the 9 *known* radio-selected SMGs with $S_{850\mu{\rm m}} \gtrsim 5$ mJy in the GOODS-N field that overlap with our near-IR imaging (Chapman et al. 2005;Wang et al. 2004). Also listed are two (pair) sources with $S_{850\mu{\rm m}} \sim 4$ mJy taken from Chapman et al. (2005) and Wang et al. (2004). Of the 7 SMGs with redshifts $1.4 < z < 2.6$, 3 satisfy the BX/BM criteria. The detection rate of $\sim 40\%$ is similar to the detection rate of SMGs with BX/BM colors found by Chapman et al. (2005). The mean bolometric luminosity of the 5 SMGs is $\langle L_{\rm bol} \rangle \sim 9 \times 10^{12}$ L$_\odot$ as inferred from their submillimeter emission, corresponding to an SFR of ~ 1500 M$_\odot$ yr^{-1} using the Kennicutt (1998) relation[7]. Despite their large bolometric luminosities, the three submillimeter galaxies with redshifts in our sample have dust-corrected UV SFRs of $14-28$ M$_\odot$ yr^{-1}. In these cases, the UV emission may come from a relatively unobscured part of the galaxy or may be scattered out of the optically-thick dusty regions (Chapman et al. 2005). The BzK/SF criteria cull 5 of the 7 SMGs with redshifts $1.4 < z < 2.6$. Therefore, at least in the small sample of SMGs examined here (irrespective of their X-ray properties), the BX/BM and BzK/SF samples host an approximately equal number of SMGs. Finally, as we show below, galaxies with the most extreme $(z-K)_{\rm AB}$ colors (i.e., $(z-K)_{\rm AB} > 3$) are red not because they are obscured by dust, but because they have little or no current star formation. It is therefore not surprising that such objects are not identified by

[6] Those BzK/SF galaxies with $G-\mathcal{R} \gtrsim 1$ and blue $U_{\rm n}-G \lesssim 1$ have optical colors that are similar to the colors expected for lower redshift ($z \lesssim 1$) galaxies (e.g., Adelberger et al. 2004). So, if these galaxies are truly low redshift galaxies, then their inferred star formation rates would be even lower.

[7] As we discuss in § 4.4, some of the submillimeter flux may be coming from accretion activity

TABLE 4. PROPERTIES OF SUBMILLIMETER GALAXIES WITH K_s-BAND DATA

α[a] (2000.0)	δ[a] (2000.0)	$S_{850\mu m}$[b] (mJy)	K_s (Vega mag)	z[c]	$f_{SB} \times 10^{-15}$[d] (erg s^{-1} cm^{-2})	$f_{HB} \times 10^{-15}$[d] (erg s^{-1} cm^{-2})	BX/BM[e]	BzK/SF[e]	DRG[e]	L_{bol}[f] ($\times 10^{12}$ L$_\odot$)
12:36:21.27	62:17:08.4	7.8 ± 1.9	20.62	1.988	...	...	yes	yes	yes	13.5
12:36:22.65	62:16:29.7	7.7 ± 1.3	19.85	2.466	...	1.14	yes	yes	no	11.6
12:36:29.13	62:10:45.8	5.0 ± 1.3	17.65	1.013	0.17	2.23	no	no	no	1.2
12:36:35.59	62:14:24.1	5.5 ± 1.4	18.62	2.005	0.21	2.48	no	yes	no	8.1
12:36:36.75	62:11:56.1	7.0 ± 2.1	18.41	0.557	1.62	2.01	no	no	no	0.12
12:36:51.76	62:12:21.3	4.6 ± 0.8	18.34	0.298	0.34	2.65	no	no	no	0.08
12:37:07.21	62:14:08.1	4.7 ± 1.5	20.05	2.484	0.09	0.91	no	no	yes	7.5
12:37:12.05	62:12:12.3	8.0 ± 1.8	20.65	2.914	0.03	0.37	no	no	yes	5.5
12:37:21.87	62:10:35.3	12.0 ± 3.9	17.59	0.979	0.05	2.11	no	no	no	0.53
12:37:11.98	62:13:25.7	4.2 ± 1.4	20.61	1.992	...	1.01	yes	yes	no	4.9
12:37:11.34	62:13:31.0	4.4 ± 1.4	18.65	1.996[g]	0.07	0.52	no	yes	no	...

[a]Radio coordinates are from Table 2 of Chapman et al. (2005). Five of these sources are also in Wang et al. (2004). The last source listed is only from Wang et al. (2004).
[b]$S_{850\mu m}$ fluxes are from Table 2 of Chapman et al. (2005). Two of the sources are measured by Chapman et al. (2005) to have $S_{850\mu m} \sim 4.6 - 4.7$ mJy, and are measured by Borys et al. (2003) and Wang et al. (2004) to have $S_{850\mu m} > 5$ mJy, and for fairness we include these in the table.
[c]Spectroscopic redshift from Chapman et al. (2005).
[d]Soft and hard band fluxes are from Alexander et al. (2003).
[e]This field indicates whether the submillimeter source satisfies the BX/BM, BzK/SF, and DRG selection criteria.
[f]Inferred bolometric luminosity from Chapman et al. (2005). The mean bolometric luminosity of the 6 submillimeter galaxies with spectroscopic redshifts $1.4 < z < 2.6$ is $\langle L_{bol} \rangle \sim 9 \times 10^{12}$ L$_\odot$.
[g]Redshift from Swinbank et al. (2004).

criteria designed to select star-forming galaxies.

4.2. *Passively Evolving Galaxies at $z \sim 2$*

Near-IR Colors

We now turn to galaxies in our samples that appear to have little or no current star formation. DRGs have SFRs that are comparable to those of BzK/SF and BX/BM galaxies with similar near-IR colors for $(z-K)_{AB} < 3$. However, stacking the 13 DRGs with $(z-K)_{AB} \geq 3$ results in a non-detection with an upper limit of ~ 50 M$_\odot$ yr^{-1} (Figure 16). Stacking the X-ray emission from the 17 BzK/PE galaxies shows a similar turnover in the inferred average SFR around $(z-K)_{AB} \sim 3$ (Figure 16). The BzK colors of the DRGs (most of which only have B-band limits) lie in the BzK color space expected for passively-evolving galaxies (Figure 12). The stacking analysis confirms that these red DRGs and BzK/PE galaxies have little current star formation compared with DRGs and BzK/PE galaxies with bluer near-IR colors (Figure 16). A similar X-ray stacking analysis by Brusa et al. (2002) yields no detection for passive EROs in the K20 survey from the *Chandra* Deep Field South data.

The average $J - K_s$ color of the 13 passively evolving DRGs (with $(z-K)_{AB} > 3$) is $\langle J-K_s \rangle = 2.98 \pm 0.59$, and is comparable to the average $J - K_s$ color of DRGs with bluer $(z-K)_{AB}$ colors, implying that the J-band is either in close proximity to the Balmer and 4000 Å breaks or the band encompasses the breaks completely. This will occur for galaxies with a mean redshift $\langle z \rangle \sim 1.88 - 2.38$ (Figure 3). In these cases, the $(z-K)_{AB}$ color will be more effective than the $J-K_s$ color in culling those galaxies with developed spectral breaks. The fraction of passively evolving DRGs inferred from their lack of X-ray emission is $13/54 \sim 24\%$, which is in reasonable agreement to the passively evolving DRG fraction of $\sim 30\%$ found by Förster Schreiber et al. (2004) and Labbé et al. (2005).

Alternatively, galaxies with $2 < (z-K)_{AB} < 3$ must still be forming stars at a prodigious rate, as indicated by their stacked X-ray flux. The similarity in average K_s magnitude between galaxies with $2 \leq (z-K)_{AB} < 3$ and $(z-K)_{AB} \geq 3$ (Figure 16) suggests they have similar masses, and the difference in $(z-K)_{AB}$ color between the two samples simply reflects the presence of some relatively unobscured star formation in those galaxies with $2 \leq (z-K)_{AB} < 3$.

Stellar Populations

Figure 18 further illustrates the differences between the star-forming and passively evolving galaxies in terms of some physical models. The left panel of Figure 18 shows the $(z-K)_{AB}$ versus $(K - m_{3.6/4.5\mu m})_{AB}$ colors (near-IR/IRAC color diagram) for all galaxies, excluding direct X-ray detections [8]. Because the SEDs of (non-AGN) galaxies considered here are expected to be relatively flat in f_ν across the IRAC bands, we used 3.6 μm IRAC AB magnitudes for all sources that were not covered by the 4.5 μm imaging. Also shown in Figure 18a are synthetic colors for Bruzual & Charlot (2003) spectral templates at the mean redshifts of the BM ($\langle z \rangle \sim 1.7$) and BX ($\langle z \rangle \sim 2.2$) samples, assuming constant star formation, $E(B-V) = 0$ and 0.3, and a Calzetti et al. (2000) reddening law. The bulk of BX/BM and BzK/SF galaxies generally fall within the region of color space expected for constant star forming galaxies with moderate extinction of $E(B-V) \sim 0.15$ and ages of ~ 1 Gyr. These values are consistent with those derived from detailed spectral modeling of BX/BM galaxies and LBGs

[8] Labbé et al. (2005) propose a similar diagram to differentiate DRGs from other (e.g., star-forming) populations of $z \sim 2$ galaxies.

by Shapley et al. (2005). Much of the scatter of star-forming galaxies to the left and right of the CSF models for $E(B-V) = 0.15-0.30$ is a result of photometric uncertainty, particularly in the $(K - m_{3.6/4.5\mu m})_{\rm AB}$ color, since we include galaxies with formal IRAC uncertainties of 0.5 mag. In addition, some of the scatter for objects with blue $(z-K)_{\rm AB}$ colors arises from interlopers. The more interesting aspect of Figure 18a is that the constant star formation models cannot account for the colors of objects with $(z-K)_{\rm AB} \gtrsim 3$: these objects must have ages less than the age of the universe at $z \sim 2$ (~ 3 Gyr) and simultaneously have modest $E(B-V)$—and hence modest current SFRs$\lesssim$ 190 M$_\odot$ yr^{-1}—such that they remain undetected as soft-band X-ray sources. The important result is that, similar to SED fitting, the X-ray stacking analysis allows us to rule out certain star formation histories. For the PE galaxies considered here, the X-ray data rule out the constant star formation models. The benefit of X-ray data is that we can quantify the current SFR independent of extinction and the degeneracies which plague SED fitting.

The only models that can account for the colors of objects with $(z-K)_{\rm AB} \gtrsim 3$ are those with declining star formation histories (right panel of Figure 18). For example, DRG/PEs at $z \sim 2.2$ have colors that can be reproduced by dust free models ($E(B-V) = 0.0$) with star formation decay timescales between $\tau = 10$ Myr (instantaneous burst) and $\tau \sim 700$ Myr[9]. While the upper limit on the current average SFRs of DRG/PEs of 50 M$_\odot$ yr^{-1} (Figure 16) does not help us further constrain the star formation history to a narrower range in τ, the fact that DRG/PEs are still detected at z-band suggests that single stellar population models with small τ are unrealistic (e.g., ages greater than 1 Gyr imply >100 e-folding times for the instantaneous burst model making such an object undetected at z-band). If there is ongoing low level star formation activity, then a two component model with a underlying old stellar population and a recent star formation episode may be required (e.g., Yan et al. 2004).

The red $(z-K)_{\rm AB} > 3$ colors of BzK/PE galaxies can be reproduced by models with $\tau \sim 10-300$ Myr (for τ much larger than 300 Myr, the models over predict the current star formation rate). The X-ray data indicate that these BzK/PE galaxies have an average current SFR of ~ 28 M$_\odot$ yr^{-1}. For an age of 1 Gyr and $\tau = 300$ Myr, this implies an "initial" SFR of ~ 800 M$_\odot$ yr^{-1} at $z \sim 2.4$. This initial SFR is comparable to that of SMGs and the implied formation redshift is close to the median redshift of SMGs ($z \sim 2.2$), suggesting SMGs could be plausible progenitors of BzK/PE galaxies if the single component model correctly described the star formation histories of these galaxies (e.g., Cimatti et al. 2004). The formation redshifts can be pushed back in time to significantly earlier epochs $z \gtrsim 3.5$ if one assumes a more physically motivated "truncated" star formation history that models the effects of feedback in halting star formation (Daddi et al. 2005). Nonetheless, the simplistic example above illustrates how X-ray estimates of the bolometric SFRs of galaxies can be combined with the results of stellar population modeling to indicate the likely progenitors of such galaxies. In summary, we have demonstrated the utility of stacked X-ray data as a powerful constraint on the results from stellar population modeling. The X-ray data indicate that galaxies with $(z-K)_{\rm AB} \gtrsim 3$ have SEDs that are consistent with declining star formation history models. Other studies also show that the SEDs of BzK/PE galaxies can be adequately described by declining star formation history models (e.g., Daddi et al. 2005). The deep X-ray data confirm these results and further allow us to constrain the current SFRs of passively evolving and star-forming galaxies independent of the degeneracies associated with stellar population modeling.

[9] We rule out ages that are greater than the age of the universe at $z \sim 2.2$, giving an upper limit on the age of ~ 3 Gyr.

Space Densities

To conclude this section, we note that objects selected by their $J-K_{\rm s}$ colors appear to include a substantial number of passively evolving galaxies at redshifts $z \gtrsim 2$ (although, as we pointed out above, the $(z-K)_{\rm AB}$ color may be a more effective means of determining *which* DRGs are passively evolving). The space density implied by the 4 BzK/PE galaxies with $(z-K)_{\rm AB} > 3$ and $K_{\rm s} < 21$ is $\sim 3 \times 10^{-5}$ Mpc^{-3}, assuming a boxcar (or top-hat) selection function between redshifts $1.4 < z < 2.0$ and an area of ~ 72.3 arcmin^2. If we include all 17 BzK/PE galaxies (i.e., including those with $(z-K)_{\rm AB} < 3$ and those four that are directly-detected in X-rays) with $K_{\rm s} < 21$, we find a space density of 1.3×10^{-4} Mpc^{-3}. Given the strong clustering observing for BzK/PE galaxies (e.g., Daddi et al. 2005), our estimate is in good agreement with the value of 1.8×10^{-4} Mpc^{-3} obtained for the Daddi et al. (2005) sample of *bona-fide* BzK/PE objects in the Hubble Ultra Deep Field (UDF), an area which is 6 times smaller than the area considered in our analysis (i.e., 12.2 arcmin^2 in Daddi et al. (2005) versus 72.3 arcmin^2 considered here).

All of the BzK/PE galaxies would have been detected with $K_{\rm s} < 21$ and $(z-K)_{\rm AB} > 3$, assuming the PE model shown in Figure 18b, if they were at the mean redshift assumed for DRG/PEs of $\langle z \rangle = 2.2$. The space density of the 13 DRG/PEs with $(z-K)_{\rm AB} > 3$ is $\sim 9 \times 10^{-5}$ to $K_{\rm s} = 21$, assuming a boxcar selection function between between redshifts $2.0 < z < 2.6$ and an area of ~ 72.3 arcmin^2. Here, we have assumed that the range in redshifts of DRG/PEs ($2.0 < z < 2.6$) is similar to that of all DRG galaxies based on the spectroscopic redshift distribution shown in Figure 1. Our estimate of the DRG/PE space density is comparable to that obtained by Labbé et al. (2005) after restricting their sample to $K_{\rm s} < 21$ (yielding 1 object over ~ 5 arcmin^2), and assuming a volume between redshifts $2.0 < z < 2.6$).

It is worth noting that the BzK/PE and DRG/PE populations appear to be highly clustered (e.g., Daddi et al. 2005, van Dokkum et al. 2004) and this will likely affect their density estimates over small volumes. While the space densities derived here are in rough agreement with other studies, our estimates have been derived over a much larger volume (by a factor of $6-14$) than any previous study and will be less susceptible to variations in density due to clustering. We caution the reader that the density estimates may still be uncertain given that the redshift distribution of DRGs with $z \gtrsim 2.6$ is not well sampled, even in the large *spectroscopic* dataset of DRGs considered here.

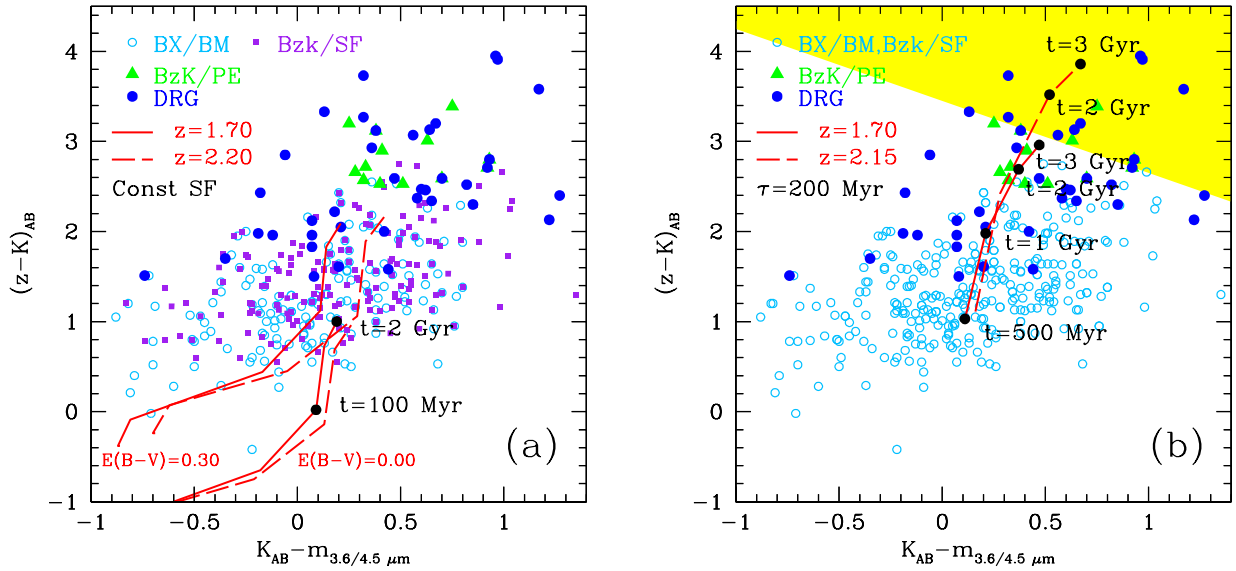

FIG. 18.— (a) $(z-K)_{\rm AB}$ versus $(K-m_{3.6/4.5\mu{\rm m}})_{\rm AB}$ colors for $K_{\rm s}<21$ galaxies in the BX/BM, BzK/SF, BzK/PE, and DRG samples. Also shown are Bruzual & Charlot (2003) spectral templates for ages 1 Myr to 3 Gyr at the mean redshifts of the BX ($\langle z\rangle\sim2.2$) and BM ($\langle z\rangle\sim1.7$) samples, assuming constant star formation, $E(B-V)=0.0$ and 0.3, and the Calzetti et al. (2000) reddening law. The models assume a Salpeter IMF from $0.1-100$ $M_\odot$ and solar metallicity. The photometric scatter is large given that we include galaxies with IRAC uncertainties up to 0.5 mag, and this accounts for the large spread in the $(K-m_{3.6/4.5\mu{\rm m}})_{\rm AB}$ colors of the star-forming candidates; (b) same as (a) except we show the spectral templates for a model with $\tau=200$ Myr and $E(B-V)=0.0$. The shaded region selects IRAC Extremely Red Objects (IEROs; Yan et al. 2004).

Taken at face value, the density estimates derived above suggest a significant presence of passively evolving $K_{\rm s}<21$ galaxies at redshifts $z\gtrsim2$. This result contrasts with that of Daddi et al. (2005) who argue for a rapid decrease in the number density of passively evolving galaxies at redshifts $z\gtrsim2$ based on BzK/PE selection. The dropoff in space density of passively evolving galaxies at redshifts $z\gtrsim2$, as suggested by Daddi et al. (2005), may be an artifact of the BzK/PE selection function which, based on previously published redshift distributions and shown in Figure 1, appears to miss passively evolving galaxies at redshifts $z\gtrsim2$, even when using the very deep B-band of this study. Figure 12 shows that all of the DRGs that cluster around the BzK/PE selection window have limits in B-band and very few actually have limits that would for certain place them in the BzK/PE window. Photometric scatter for those galaxies with very faint (or no) B-band detections is likely to be significant for these galaxies. These results suggest that the depth of the B-band data is the determining factor in whether BzK/PE selection culls galaxies with redshifts $z\gtrsim2$ or not. Because the depth of the photometry is an issue for the BzK/PE selection, it becomes difficult to accurately quantifying with a single selection criteria the dropoff in space density of passively evolving galaxies between $z\lesssim2$ and $z>2$. We can avoid the need for excessively deep B-band data to select passively evolving galaxies with redshifts $z\gtrsim2$ by simply selecting them using a single color, $J-K_{\rm s}$ or $(z-K)_{\rm AB}$. The stacked X-ray results show that a subsample of DRGs have very little star formation, suggesting that passively evolving galaxies have a significant presence at epochs earlier than $z=2$. The inferred ages of DRGs would imply formation redshifts of $z\sim5$ (Labbé et al. 2005).

We conclude this section by noting that there are several galaxies in the HS1700+643 sample of Shapley et al. (2005), and many more in optically selected samples in general (e.g., Erb et al. 2005), which have old ages and early formation redshifts similar to those of the passively evolving BzK/PE and DRG/PE galaxies discussed here. In order to reproduce the observed SEDs for such objects, the current SFR must be much smaller (but still detectable in the case of optically selected galaxies) than the past average SFR.

4.3. *Selecting Massive Galaxies*

As discussed above, DRGs with $(z-K)_{\rm AB}>3$ appear to be passively evolving based on their (lack of) stacked X-ray flux and their colors with respect to models with declining star formation histories. The X-ray data indicate that BzK/PE galaxies also appear to be well described by declining star formation histories, consistent with the SED modeling results of Daddi et al. (2005). The stellar mass estimates of these PE galaxies will be presented elsewhere. Here, we simply mention that several existing studies of the stellar populations of BzK/PE and DRG galaxies with $K_{\rm s}<20$ indicate they have masses $\gtrsim10^{11}$ $M_\odot$ (e.g., Daddi et al. 2005, Förster Schreiber et al. 2004). In addition, Yan et al. (2004) recently analyzed the stellar populations of IRAC-selected Extremely Red Objects (IEROs), selected to have $f_\nu(3.6\mu{\rm m})/f_\nu({\rm z}_{850})>20$ (or, equivalently, $(z-3.6\mu{\rm m})_{\rm AB}>3.25$). Spectral modeling indicates these sources lie at redshifts $1.6<z<2.9$, are relatively old ($1.5-3.5$ Gyr), and require an evolved stellar population to fit the observed SEDs. Almost all of the PE galaxies with $(z-K)_{\rm AB}>3$ satisfy the IERO criteria (shaded region of Figure 18b). Furthermore, the $\mathcal{R}$-band detections and limits for PEs with $(z-K)_{\rm AB}>3$ imply $\mathcal{R}-K_{\rm s}\gtrsim5.3$, satisfying the ERO criteria.

The inferred stellar masses of the Shapley et al. (2005) sample of optically-selected galaxies in the HS1700+643 field are shown in Figure 19. For comparison, we also show the inferred stellar masses from the Yan et al. (2004) sample of IEROs[10]. Both the Shapley et al. (2005) and Yan et al. (2004) samples take advantage of the longer wavelength IRAC data to constrain the stellar masses, and the typical uncertainty in mass is $\sim 40\%$ for objects with $M^* < 10^{11}$ M$_\odot$ and $\leq 20\%$ for objects with $M^* > 10^{11}$ M$_\odot$. The IERO stellar masses have been multiplied by 1.7 to convert from a Chabrier to Salpeter IMF. The scatter in Figure 19 reflects the large ($\gtrsim 1$ magnitude) variation in the mass-to-light (M/L) ratio for objects with a given rest-frame optical luminosity in the BX and IERO samples. For magnitudes brighter than our DRG completeness limit of $K_s = 21$, $\sim 16\%$ of BX galaxies have stellar masses $M^* > 10^{11}$ M$_\odot$. For $K_s < 20$ BX galaxies, the fraction with $M^* > 10^{11}$ M$_\odot$ is $\sim 40\%$. So, while optically-selected BX galaxies have a lower *mean* stellar mass than IEROs, there is certainly a subsample of BX galaxies which have masses comparable to the most massive IERO galaxies. We note that the stellar mass distributions of $K_s > 21$ BXs and IEROs do not overlap: the $\mathcal{R} - K_s$ colors of IEROs are too red for them to be included in the optically-selected sample.

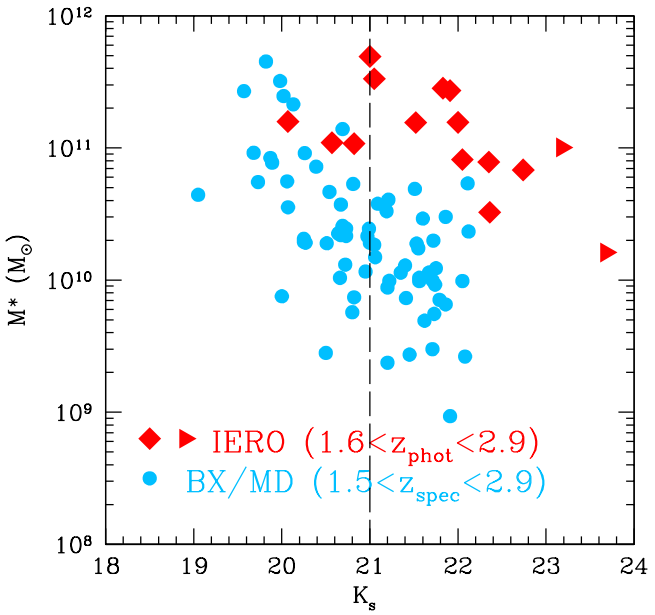

FIG. 19.— Inferred stellar masses of BX and "MD" objects from the Shapley et al. (2005) sample with spectroscopic redshifts $1.5 < z_{\rm spec} < 2.9$ (circles), and IEROs from the Yan et al. (2004) sample with photometric redshifts $1.6 < z_{\rm phot} < 2.9$ (squares, and triangles for those with K_s-band limits). The stellar masses from Yan et al. (2004) have been multiplied by 1.7 to convert from a Chabrier to Salpeter IMF. The dashed vertical line denotes the limit brighter than which we are complete for IEROs (i.e., those DRGs with $(z-K)_{\rm AB} > 3$). A subset of BX galaxies have stellar masses similar to those of the IERO sample. The scatter in stellar masses reflects at least a magnitude variation in the M/L ratio of BX/MD and IERO objects at a given rest-frame optical luminosity.

The X-ray stacking results indicate that BX/BM galaxies with $K_s < 20$ have prodigious star formation rates, while IEROs (i.e., those DRGs with $(z-K)_{\rm AB} > 3$) have very little star formation. Therefore, a simple interpretation is that optical surveys include objects that are as massive ($M^* > 10^{11}$ M$_\odot$) as those selected in near-IR surveys, with the only requirement that the galaxies have some unobscured star formation. The range of star formation rates (uncorrected for extinction) found for BX/BM galaxies is $3 - 60$ M$_\odot$ yr^{-1}, and it is likely that massive galaxies with at least a little unobscured star formation can be BX/BM selected. This may be the only significant difference between optical and near-IR selected massive galaxies, and the difference in SFR may be temporal. These criteria typically fail to select passively evolving galaxies at $z \sim 2$ as they have already settled to a quiescent stage. This does not mean that such massive galaxies will never appear in optical surveys. For example, a subsequent accretion event at $z < 2$ could elevate the star formation activity in an otherwise passively evolving massive galaxy, thus bringing it into the optical sample. Nonetheless, the DRG and BzK/PE criteria add to the census of galaxies at $z \sim 2$ by selecting passively evolving galaxies that have stellar masses similar to the most massive galaxies selected in the rest-frame UV.

4.4. *Star Formation Rate Density at $z \sim 2$*

Contribution from Optical and Near-IR Selected Samples

We can roughly estimate the contribution of BX/BM, BzK/SF, and DRG/SF galaxies to the extinction-free star formation rate density (SFRD) at $z \sim 2$[11]. The BzK/SF criteria are designed to select galaxies with redshifts $1.4 < z < 2.6$. The similarity in surface densities, volumes probed, and SFRs of galaxies in the BzK/SF and BX/BM samples implies that their contribution to the SFRD will be comparable for objects with $K_s < 22$. The redshift distribution of $K_s < 21$ DRGs from within our own sample is reasonably well defined over this redshift range (cf., Figure 1), so we can estimate the added contribution of $\sim 80\%$ of the DRGs with redshifts $2.0 \lesssim z < 2.6$ to the SFRD between redshifts $1.4 < z < 2.6$. Figure 20 and Table 5 show the cumulative contribution to the SFRD of BzK/SF, BX/BM, and DRG/SF galaxies. The points in Figure 20 are not independent of each other due to the overlap between the samples (e.g., Figure 10). Also shown in Figure 20 by the shaded region is the inferred total SFRD assuming the overlap fractions of Figure 10 and counting all objects once. The results indicate that BX/BM selection would miss approximately one-third of the total SFRD from BX/BM and BzK/SF galaxies to $K_s = 22$ and DRG/SF $K_s < 21$ galaxies combined. We remind the reader that much of the incompleteness of the BX/BM sample with respect to that of the BzK/SF sample (and vice versa) results from photometric scattering (e.g., Figures 11 and 12). Monte Carlo simulations can be used to quantify the biases of such photometric inaccuracy and thus correct for incompleteness (e.g., Reddy et al. 2005). The total SFRD in the interval $1.4 < z < 2.6$ for BX/BM

[10] H. Yan, private communication

[11] Although the BzK/PE galaxies do have detectable X-ray emission (e.g., Figure 16), their contribution to the SFRD is minimal given that their space density is a factor of 5 smaller than that of the BzK/SF and BX/BM galaxies to $K_s = 21$ in the redshift range $1.4 < z < 2.0$.

TABLE 5. CUMULATIVE CONTRIBUTIONS TO THE SFRD BETWEEN $1.4 < z < 2.6$

K_s Range	Sample[a]	z[b]	ρ[c] (arcmin^{-2})	SFRD[d] ($M_\odot$ yr^{-1} Mpc^{-3})
$K_s \leq 20.0$	BX/BM	1.4–2.6	0.44	0.016 ± 0.008
	BzK/SF	1.4–2.6	0.62	0.018 ± 0.004
	DRG/SF	2.0–2.6	0.15	0.008 ± 0.002
	BzK/SF—BX/BM	1.4–2.6	0.35	0.007 ± 0.002
	DRG/SF—BzK/SF—BX/BM	2.0–2.6	0.08	0.004 ± 0.001
	Total	2.0–2.6	0.87	0.027 ± 0.006
$K_s \leq 20.5$	BX/BM	1.4–2.6	1.13	0.034 ± 0.009
	BzK/SF	1.4–2.6	1.35	0.032 ± 0.006
	DRG/SF	2.0–2.6	0.30	0.013 ± 0.003
	BzK/SF—BX/BM	1.4–2.6	0.55	0.012 ± 0.002
	DRG/SF—BzK/SF—BX/BM	2.0–2.6	0.25	0.009 ± 0.002
	Total	2.0–2.6	1.93	0.055 ± 0.011
$K_s \leq 21.0$	BX/BM	1.4–2.6	2.15	0.045 ± 0.010
	BzK/SF	1.4–2.6	2.34	0.044 ± 0.009
	DRG/SF	2.0–2.6	0.58	0.020 ± 0.004
	BzK/SF—BX/BM	1.4–2.6	0.74	0.014 ± 0.002
	DRG/SF—BzK/SF—BX/BM	2.0–2.6	0.41	0.013 ± 0.002
	Total	2.0–2.6	3.30	0.072 ± 0.014
$K_s \leq 21.5$	BX/BM	1.4–2.6	3.17	0.057 ± 0.013
	BzK/SF	1.4–2.6	3.61	0.052 ± 0.010
	BzK/SF—BX/BM	1.4–2.6	1.71	0.017 ± 0.002
	Total[e]	2.0–2.6	5.29	0.087 ± 0.017
$K_s \leq 22.0$	BX/BM	1.4–2.6	4.31	0.069 ± 0.015
	BzK/SF	1.4–2.6	4.93	0.068 ± 0.014
	BzK/SF—BX/BM	1.4–2.6	2.55	0.020 ± 0.003
	Total[e]	2.0–2.6	7.27	0.102 ± 0.021

[a]The BzK/SF—BX/BM sample represents the set of objects that are BzK/SF-selected, but not BX/BM-selected. Similarly, the DRG/SF—BzK/SF—BX/BM sample represents the set of DRGs that are not selected by either the BzK/SF or BX/BM criteria.
[b]Redshift range of sample.
[c]Surface density of photometric objects after removing interlopers and directly detected X-ray sources that are likely AGN. The number of BX/BM objects is calculated assuming the spectroscopic and interloper fractions from Table 1. The overlap fractions are taken from Figure 10. We assume a field area of ~ 72.3 arcmin^2 to compute surface densities.
[d]Assumes the average SFRs shown in Figure 15.
[e]This includes the contribution from the DRG/SF—BzK/SF—BX/BM sample for $K_s < 21$.

and BzK/SF galaxies to $K_s = 22$ and DRG/SF galaxies to $K_s = 21$, taking into account the overlap between the samples, is $\sim 0.10 \pm 0.02$ $M_\odot$ yr^{-1} Mpc^{-3}. Approximately 30% of this comes from galaxies with $K_s < 20$ (Table 5). Optically-selected galaxies to $\mathcal{R} = 25.5$ and $K_s = 22.0$ and BzK/SF galaxies to $K_s = 22.0$ (with significant overlap between the two samples) account for $\sim 87\%$ of the total SFRD quoted above. DRGs to $K_s = 21$ that are not selected by the BX/BM or BzK/SF criteria contribute the remaining $\sim 13\%$. We note that the number $\sim 0.10 \pm 0.02$ $M_\odot$ yr^{-1} Mpc^{-3} does not include the 5 radio-selected SMGs to $S_{850\mu m} \gtrsim 5$ mJy that are near-IR and/or optically-selected since we removed the directly-detected hard-band X-ray sources in computing the SFRD. If we add these 5 radio-selected SMGs that are present in the optical and near-IR samples (all of which have $K_s < 21$), then the total SFRD contributed by the BX/BM and BzK/SF objects to $K_s = 22.0$ and DRG/SF galaxies to $K_s = 21.0$ is $\sim 0.15 \pm 0.03$ $M_\odot$ yr^{-1} Mpc^{-3} (see next section).

Contribution from Radio-Selected Submillimeter Galaxies

We conclude this section by briefly considering the contribution of radio-selected submillimeter galaxies (SMGs) with $S_{850\mu m} \gtrsim 5$ mJy to the SFRD. All but one of the radio-selected SMGs summarized in Table 4 are directly detected in either the soft or hard band and are likely associated with AGN. Stacking the X-ray emission for the 5 radio-selected SMGs with redshifts $1.4 < z < 2.6$ in Table 4 yields an average inferred SFR of ~ 2900 $M_\odot$ yr^{-1}, and this value should be regarded as an upper limit given that the X-ray emission is likely contaminated by AGN. On the other hand, the average bolometric luminosity of the 5 SMGs, as derived from their submillimeter flux, is $\langle L_{bol} \rangle \sim 9 \times 10^{12}$ $L_\odot$. If we assume that 30% of L_{bol} arises from AGN (e.g., Chapman et al. 2005, Alexander et al. 2005), then the implied SFR is ~ 1000 $M_\odot$ yr^{-1}. If we take at face value the assertion that 30% of the bolometric luminosity of submillimeter galaxies comes from AGN, then this means the X-ray emission would overestimate the average SFR of SMGs by a factor of ~ 3. In other words, only one-third of the X-ray emission from SMGs would result from star-formation, and the remaining two-thirds would come from AGN.

To determine the *additional* SFRD provided by radio-selected SMGs with $S_{850\mu m} \gtrsim 5$ mJy, we must account for their overlap with the optical and near-IR samples. The data in Table 4 show that there are 4 of 9 SMGs that

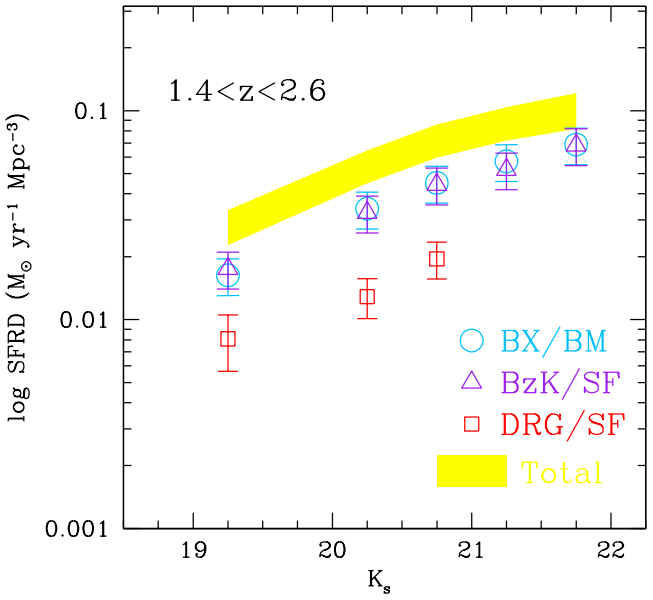

FIG. 20.— *Cumulative* star formation rate density (SFRD) as a function of K_s magnitude for BX/BM (circles), BzK/SF (triangles), and DRG/SF (squares) galaxies with redshifts $1.4 < z < 2.6$. The points are not independent of each other given the overlap between the samples. The shaded region denotes the total cumulative SFRD when counting overlap objects once. The total SFRD to $K_s = 22$ includes DRGs with $K_s < 21$. The error bars reflect the Poisson error and uncertainty in star formation rate added in quadrature, but do not reflect systematic errors associated with, e.g., photometric scattering.

are not selected by the optical and/or near-IR criteria. All 4 of these galaxies have relatively low redshifts $z \lesssim 1$ and will obviously not contribute to the SFRD between redshifts $1.4 < z < 2.6$. Alternatively, of the 5 SMGs that are spectroscopically confirmed to lie at redshifts $1.4 < z < 2.6$, *all* are selected by either the BX/BM, BzK/SF, or DRG criteria (and sometimes by more than one set of criteria).

Because of the non-uniform coverage of the submillimeter observations, we must rely on the published submillimeter number counts to estimate the effective surface density probed by the 9 radio-selected SMGs with $S_{850\mu m} \gtrsim 5$ mJy listed in Table 4. According to the models shown in Figure 4 of Smail et al. (2002), we should expect to find ~ 0.25 sources arcmin^{-2} to $S_{850\mu m} \sim 5$ mJy. Neglecting cosmic variance, the nine observed radio-selected SMGs to $S_{850\mu m} \sim 5$ mJy then imply an effective surface area of ~ 36 arcmin^2. The spectroscopic redshifts compiled in Table 2 of Chapman et al. (2005) indicate that $\approx 44\%$ of the radio-selected SMGs to $S_{850\mu m} \sim 5$ mJy lie at redshifts outside the range $1.4 < z < 2.6$. If we assume a Poisson distribution of sources, then the total number of SMGs to $S_{850\mu m} \sim 5$ mJy could be as high $9 + \sqrt{9} = 12$. If we assume that the fraction of interlopers among the 3 unobserved objects is similar to the fraction of interlopers among objects which are observed, then we expect an upper limit of two SMGs with $S_{850\mu m} \sim 5$ mJy that are unobserved and that lie between redshifts $1.4 < z < 2.6$. If we conservatively assume that these two sources are not selected by the optical and/or near-IR criteria, and they have bolometric SFRs of ~ 1500 M$_\odot$ yr^{-1} (similar to the average SFR found for the 5 spectroscopically confirmed radio-selected SMGs in Table 4), then the inferred *additional* SFRD provided by these two SMGs would be ~ 3000 M$_\odot$ yr^{-1} divided by the volume subtended by 36 arcmin^2 at redshifts $1.4 < z < 2.6$, or ~ 0.022 M$_\odot$ yr^{-1} Mpc^{-3}. We note that this should be treated as an upper limit for several reasons. First, we have assumed the maximum number of unobserved sources allowed by Poisson statistics. Second, we have assumed an interloper fraction among these unobserved sources that is the same for the observed sources. In general, one might expect the contamination fraction to be higher among the general SMG population to $S_{850\mu m} \sim 5$ mJy (where an accurate radio position may not be known) than would be inferred from the radio-selected SMG surveys. Finally, we have assumed that all of the unobserved sources cannot be selected by their optical and/or near-IR colors. Neglecting any overlap, radio-selected SMGs to $S_{850\mu m} \sim 5$ mJy contribute ~ 0.05 M$_\odot$ yr^{-1} Mpc^{-3} to the SFRD between redshifts $1.4 < z < 2.6$. However, our conservative calculation indicates that radio-selected SMGs to $S_{850\mu m} \sim 5$ mJy that are not selected by optical (BX/BM) and/or near-IR (BzK and/or DRG) surveys make a small ($\lesssim 0.022$ M$_\odot$ yr^{-1} Mpc^{-3} or $\lesssim 15\%$) *additional* contribution to the SFRD between redshifts $1.4 < z < 2.6$.

5. CONCLUSIONS

We have taken advantage of the extensive multi-wavelength data in the GOODS-North field to select galaxies at $z \sim 2$ based on their optical and near-IR colors and to compare them in a consistent manner. Our own ground-based optical and near-IR images are used to select galaxies based on their $U_nG\mathcal{R}$, BzK, and $J-K_s$ colors. Additional rest-frame UV spectroscopy for 25% of optically selected candidates allows us to quantify the redshift selection functions for the various samples. We use the deep *Chandra* 2 Ms X-ray data to determine the influence of AGN and estimate bolometric SFRs for galaxies in the optical and near-IR samples. We also use the deep *Spitzer*/IRAC data in the GOODS-North field in considering the stellar populations and masses of galaxies selected in different samples. Our analysis employs the same multi-wavelength data for a single field (GOODS-North), using the same photometric measurement techniques, for a consistent comparison between galaxies selected by their optical and near-IR colors. Our main conclusions are as follows:

1. Star-forming galaxies at $z \sim 2$ selected by their $U_nG\mathcal{R}$ colors (i.e., BX/BM galaxies) and their BzK colors (i.e., BzK/SF galaxies) have optical and near-IR color distributions that indicate significant overlap ($\sim 70 - 80\%$) between the two samples. Photometric scatter could account for the colors of at least half of those galaxies missed by one set of criteria or the other. The BzK/SF criteria are less efficient in selecting (younger) $K_s > 21$ galaxies at redshifts $1.4 < z < 2.6$, while the BX/BM criteria are less efficient in selecting near-IR bright (e.g., $K_s < 20$) objects. Distant red galaxies (DRGs; including both reddened star-forming and passively evolving galaxies) selected to have $J-K_s > 2.3$ show near-IR colors that are $1 - 1.5$ magnitudes redder than for samples of star-forming galaxies. Criteria aimed at selecting passively evolving galaxies based on their

BzK colors (i.e., BzK/PE galaxies) by design have red near-IR colors, but we find that the redshift distributions of BzK/PE galaxies and DRGs have very little overlap.

2. The deep X-ray data show that almost all of the directly detected X-ray sources in the samples have hard band emission and X-ray/optical flux ratios indicating they are likely AGN. Much of this AGN contamination occurs for magnitudes $K_s < 20$. We identify 5 objects that are detected in the soft band X-ray data and are likely star-forming galaxies based on their absence in the hard-band X-ray data, optical magnitudes $R > 22$, and absence of obvious AGN features for those with spectra. We stacked the X-ray data for all likely star-forming galaxies (i.e., those undetected in X-rays and the 5 galaxies discussed above), excluding likely AGN. The stacking analysis shows that the star formation rate (SFR) distributions of BX/BM and BzK/SF galaxies and DRGs are very similar as a function of K_s magnitude. Galaxies with $K_s < 20$ have average SFRs of ~ 120 $M_\odot$ yr^{-1}, a factor of two to three higher than $K_s > 20.5$ galaxies. Previous studies point to a similarity in the metallicities, clustering, and stellar masses of $K_s < 20$ optical and near-IR selected galaxies (e.g., Shapley et al. 2004, Adelberger et al. 2005). In this work we show that the bolometric SFRs of optical and near-IR selected galaxies are also very similar when subjected to a common near-IR magnitude.

3. Near-IR selection of star forming galaxies should be more immune to the effects of dust obscuration than optical surveys. However, the BX/BM, BzK/SF, and DRG samples show very similar SFRs as a function of near-IR color for galaxies with $(z-K)_{AB} < 3$. The SFRs inferred for BzK/SF galaxies which are not optically-selected are very similar to BzK/SF galaxies which do satisfy the optical criteria, suggesting that star-forming galaxies in near-IR samples that are missed by optical criteria do not harbor large numbers of heavily reddened galaxies. Furthermore, the optical and BzK/SF samples host an approximately equal number of submillimeter galaxies (SMGs). Despite their very high SFRs (~ 1000 $M_\odot$ yr^{-1}), SMGs missed by optical and near-IR selection have insufficient space densities to make a significant contribution ($\lesssim 10\%$, see conclusion 6 below) to the total census of star formation at redshifts $1.4 \lesssim z \lesssim 2.6$.

4. We identify a population of extremely red BzK and DRG galaxies with $(z-K)_{AB} \gtrsim 3$. The stacked X-ray data indicate these red galaxies have little, if any, current star formation. The absence of X-ray emission from these objects also suggests that low luminosity AGN and low mass X-ray binaries contribute little X-ray emission in star-forming galaxies compared with the emission produced from more direct tracers of the current star formation rate, such as high mass X-ray binaries. We further demonstrate the utility of deep X-ray data to constrain the stellar populations of these extremely red galaxies, and find that they must be described by declining star formation histories. Almost all of these passively evolving galaxies satisfy the IERO criteria of Yan et al. (2004). We find that optical selection includes a subset of galaxies with stellar masses similar to those inferred for IEROs, but which are forming stars at a prodigious rate. The stellar mass estimates from SED modeling (e.g., Yan et al. 2004, Förster Schreiber et al. 2004) and bolometric SFR estimates from the deep X-ray data (this work) suggest that the presence or absence of star formation may be the only significant difference between optical and near-IR selected massive galaxies ($M^* > 10^{11}$ $M_\odot$), and the difference in SFR may be temporal.

5. We find evidence for a significant presence of passively evolving galaxies at redshifts $z \gtrsim 2$ compared with their space density at lower redshifts, $1.4 < z < 2.0$. Our analysis suggests that a single color technique using the $(z-K)_{AB}$ or $J-K_s$ color allows for a more practical method selecting passively evolving galaxies with $z \gtrsim 2$ than the BzK/PE criteria, as the latter would require excessively deep B-band data to accurately determine the space densities of passively evolving galaxies at $z \gtrsim 2$.

6. Finally, we consider the contribution of optical and near-IR selected galaxies to the SFRD at $z \sim 2$, taking into account the overlap between the samples and their respective redshift distributions. We find that BX/BM and BzK/SF galaxies to $K_s = 22$, and DRG galaxies to $K_s = 21$, account for an SFRD of $\sim 0.10 \pm 0.02$ $M_\odot$ yr^{-1} Mpc^{-3} between redshifts $1.4 < z < 2.6$. Approximately 87% of this total comes from optically-selected galaxies to $\mathcal{R} = 25.5$ and $K_s = 22$ and near-IR selected BzK galaxies to $K_s = 22$, and 13% from $K_s < 21$ DRGs not selected by the BX/BM or BzK criteria. Of the known radio-selected SMGs to $S_{850\mu m} \sim 4$ mJy in the GOODS-N field with redshifts $1.4 < z < 2.6$, $\gtrsim 80\%$ could be selected by the BX/BM, BzK, and/or DRG criteria.

We thank Scott Chapman for discussions regarding submillimeter galaxies in the GOODS-North field. Haojing Yan kindly provided stellar mass estimates for IEROs. We thank David Alexander for his suggestions regarding the use of the X-ray data, and Amy Barger for her comments regarding Table 4. NAR, DKE, and CCS are supported by grant AST 03-07263 from the National Science Foundation and by the David and Lucile Packard Foundation. AES and KLA are supported by the Miller Foundation and the Carnegie Institute of Washington, respectively.

REFERENCES

Abraham, R. G., Glazebrook, K., McCarthy, P. J., Crampton, D., Murowinski, R., Jørgensen, I., Roth, K., Hook, I. M., Savaglio, S., Chen, H., Marzke, R. O., & Carlberg, R. G. 2004, AJ, 127, 2455

Adelberger, K. L., Erb, D. K., Steidel, C. C., Reddy, N. A., Pettini, M., & Shapley, A. E. 2005, ApJ, 620, L75

Adelberger, K. L., Steidel, C. C., Shapley, A. E., Hunt, M. P., Erb, D. K., Reddy, N. A., & Pettini, M. 2004, ApJ, 607, 226

Adelberger, K. L. & Steidel, C. C. 2000, ApJ, 544, 218

Alexander, D. M., Bauer, F. E., Chapman, S. C., Smail, I., Blain, A. W., Brandt, W. N., & Ivison, R. J. 2005, submitted to ApJ

Alexander, D. M., Bauer, F. E., Brandt, W. N., Schneider, D. P., Hornschemeier, A. E., Vignali, C., Barger, A. J., Broos, P. S., Cowie, L. L., Garmire, G. P., Townsley, L. K., Bautz, M. W., Chartas, G., & Sargent, W. L. W. 2003, AJ, 126, 539

Barger, A. J., Cowie, L. L., Capak, P., Alexander, D. M., Bauer, F. E., Fernandez, E., Brandt, W. N., Garmire, G. P., & Hornschemeier, A. E. 2003, AJ, 126, 632

Borys, C. and Chapman, S. and Halpern, M. & Scott, D. 2003, MNRAS, 344, 385
Brusa, M., Comastri, A., Daddi, E., Cimatti, A., Mignoli, M., & Pozzetti, L. 2002, ApJ, 581, L89
Bruzual, G. & Charlot, S. 2003, MNRAS, 344, 1000
Calzetti, D., Armus, L., Bohlin, R. C., Kinney, . A. L., Koornneef, J., & Storchi-Bergmann, T. 2000, ApJ, 533, 682
Capak, P., Cowie, L. L., Hu, E. M., Barger, A. J., Dickinson, M., Fernandez, E., Giavalisco, M., Komiyama, Y., Kretchmer, C., McNally, C., Miyazaki, S., Okamura, S., & Stern, D. 2004, AJ, 127, 180
Chapman, S. C., Blain, A. W., Smail, I., & Ivison, R. J. 2005, ApJ, 622, 772
Cimatti, A., Daddi, E., Renzini, A., Cassata, P., Vanzella, E., Pozzetti, L., Cristiani, S., Fontana, A., Rodighiero, G., Mignoli, M., & Zamorani, G. 2004, Nature, 430, 184
Cimatti, A., Mignoli, M., Daddi, E., Pozzetti, L., Fontana, A., Saracco, P., Poli, F., Renzini, A., Zamorani, G., Broadhurst, T., Cristiani, S., D'Odorico, S., Giallongo, E., Gilmozzi, R., & Menci, N. 2002a, A&A, 392, 395
Cimatti, A., Pozzetti, L., Mignoli, M., Daddi, E., Menci, N., Poli, F., Fontana, A., Renzini, A., Zamorani, G., Broadhurst, T., Cristiani, S., D'Odorico, S., Giallongo, E., & Gilmozzi, R. 2002b, A&A, 391, L1
Daddi, E., Cimatti, A., Renzini, A., Fontana, A., Mignoli, M., Pozzetti, L., Tozzi, P., & Zamorani, G. 2004a, ApJ, 617, 746
Daddi, E., Cimatti, A., Renzini, A., Vernet, J. ., Conselice, C., Pozzetti, L., Mignoli, M., Tozzi, P. an d Broadhurst, T., di Serego Alighieri, S., Fontana, A., Nonino, M., Rosati, P., & Zamorani, G. 2004b, ApJ, 600, L127
Daddi, E., Renzini, A., Pirzkal, N., Cimatti, A., Malhotra, S., Stiavelli, M., Xu, C., Pasquali, A., Rhoads, J., Brusa, M., Di Serego Alighieri, S., Ferguson, H., Koekemoer, A., Moustakas, L., Panagia, N., & Windhorst, R. 2005, astro-ph/0503102
Diplas, A. & Savage, B. D. 1994, ApJS, 93, 211
Erb, D. K., Steidel, C. C., Shapley, A. E., Reddy, N. A., Adelberger, K. L., & Pettini, M. 2005, in preparation
Förster Schreiber, N. M., van Dokkum, P. G., Franx, M., Labbé, I., Rudnick, G., Daddi, E., Illingworth, G. D., Kriek, M., Moorwood, A. F. M., Rix, H.-W., Röttgering, H., Trujillo, I., van der Werf, P., van Starkenburg, L., & Wuyts, S. 2004, ApJ, 616, 40
Feigelson, E. D., Broos, P., Gaffney, J. A., Garmire, G., Hillenbrand, L. A., Pravdo, S. H., Townsley, L., & Tsuboi, Y. 2002, ApJ, 574, 258
Franx, M., Labbé, I., Rudnick, G., van Dokkum , P. G., Daddi, E., Förster Schreiber, N. M., Moorwood, A., Rix, H., Röttgering, H., van de Wel, A., van der Werf, P., & van Starkenburg, L. 2003, ApJ, 587, L79
Frayer, D. T., Chapman, S. C., Yan, L., Armus, L., Helou, G., Fadda, D., Morganti, R., Garrett, M. A., Appleton, P., Choi, P., Fang, F., Heinrichsen, I., Im, M., Lacy, M., Marleau, F., Masci, F. J., Shupe, D. L., Soifer, B. T., Squires, G. K., Storrie-Lombardi, L. J., Surace, J. A., Teplitz, H. I., & Wilson, G. 2004, ApJS, 154, 137
Giavalisco, M., Ferguson, H. C., Koekemoer, A. M., Dickinson, M., Alexander, D. M., Bauer, F. E., Bergeron, J., Biagetti, C., Brandt, W. N., Casertano, S., Cesarsky, C., Chatzichristou, E., Conselice, C., Cristiani, S., Da Costa, L., Dahlen, T., de Mello, D., Eisenhardt, P., Erben, T., Fall, S. M., Fassnacht, C., Fosbury, R., Fruchter, A., Gardner, J. P., Grogin, N., Hook, R. N., Hornschemeier, A. E., Idzi, R., Jogee, S., Kretchmer, C., Laidler, V., Lee, K. S., Livio, M., Lucas, R., Madau, P., Mobasher, B., Moustakas, L. A., Nonino, M., Padovani, P., Papovich, C., Park, Y., Ravindranath, S., Renzini, A., Richardson, M., Riess, A., Rosati, P., Schirmer, M., Schreier, E., Somerville, R. S., Spinrad, H., Stern, D., Stiavelli, M., Strolger, L., Urry, C. M., Vandame, B., Williams, R., & Wolf, C. 2004, ApJ, 600, L93
Glazebrook, K., Abraham, R. G., McCarthy, P. J., Savaglio, S., Chen, H., Crampton, D., Murowinski, R., Jørgensen, I., Roth, K., Hook, I., Marzke, R. O., & Carlberg, R. G. 2004, Nature, 430, 181
Grimm, H.-J., Gilfanov, M., & Sunyaev, R. 2002, A&A, 391, 923
Hornschemeier, A. E., Brandt, W. N., Garmire, G. P., Schneider, D. P., Barger, A. J., Broos, P. S., Cowie, L. L., Townsley, L. K., Bautz, M. W., Burrows, D. N., Chartas, G., Feigelson, E. D., Griffiths, R. E., Lumb, D., Nousek, J. A., Ramsey, L. W., & Sargent, W. L. W. 2001, ApJ, 554, 742
Kauffmann, G., Heckman, T. M., Tremonti, C., Brinchmann, J., Charlot, S., White, S. D. M., Ridgway, S. E., Brinkmann, J., Fukugita, M., Hall, P. B., Ivezić, Ž., Richards, G. T., & Schneider, D. P. 2003, MNRAS, 346, 1055
Kennicutt, R. C. 1998, ARA&A, 36, 189
Labbé, I., Huang, J., Franx, M., Rudnick, G., Barmby, P., Daddi, E., van Dokkum, P. G., Fazio, G. G., Förster Schreiber, N. M., Moorwood, A. F. M., Rix, H.-W., Röttgering, H., Trujillo, I., & van der Werf, P. 2005, astro-ph/0504219
Laird, E., Nandra, K., Adelberger, K. L., Steidel, C. C., & Reddy, N. A. 2005, astro-ph/0501411
Meurer, G. R., Heckman, T. M., & Calzetti, D. 1999, ApJ, 521, 64
Nandra, K., Mushotzky, R. F., Arnaud, K., Steidel, C. C., Adelberger, K. L., Gardner, J. P., Teplitz, H. I., & Windhorst, R. A. 2002, ApJ, 576, 625
Oke, J. B., Cohen, J. G., Carr, M., Cromer, J., Dingizian, A., Harris, F. H., Labrecque, S., Lucinio, R., Schaal, W., Epps, H., & Miller, J. 1995, PASP, 107, 375
Ranalli, P., Comastri, A., & Setti, G. 2003, A&A, 399, 39
Reddy, N. A., Adelberger, K. L., Steidel, C. C., Shapley, A., Pettini, M., & Erb, D. K. 2005, ApJ, submitted
Reddy, N. A. & Steidel, C. C. 2004, ApJ, 603, L13
Rubin, K. H. R., van Dokkum, P. G., Coppi, P., Johnson, O., Förster Schreiber, N. M., Franx, M., & van der Werf, P. 2004, ApJ, 613, L5
Seibert, M., Heckman, T. M., & Meurer, G. R. 2002, AJ, 124, 46
Shapley, A., Steidel, C. C., Erb, D. K., Reddy , N. A., Adelberger, K. L., & Pettini, M. 2005, astro-ph/0503485
Shapley, A. E., Erb, D. K., Pettini, M., Steidel, C. C., & Adelberger, K. L. 2004, ApJ, 612, 108
Smail, I. and Ivison, R. J. and Blain, A. W. & Kneib, J.-P. 2002, MNRAS, 331, 495
Stark, A. A., Gammie, C. F., Wilson, R. W., Bally, J., Linke, R. A., Heiles, C., & Hurwitz, M. 1992, ApJS, 79, 77
Steidel, C. C., Adelberger, K. L., Shapley, A. E., Pettini, M., Dickinson, M., & Giavalisco, M. 2003, ApJ, 592, 728
Steidel, C. C., Shapley, A. E., Pettini, M., Adelberger, K. L., Erb, D. K., Reddy, N. A., & Hunt, M. P. 2004, ApJ, 604, 534
Strickland, D. K., Heckman, T. M., Colbert, E. J. M., Hoopes, C. G., & Weaver, K. A. 2004, ApJ, 606, 829
Swinbank, A. M. and Smail, I. and Chapman, S. C. and Blain, A. W. and Ivison, R. J. and Keel, W. C. 2004, ApJ, 617, 64
van Dokkum, P. G., Förster Schreiber, N. M., Franx, M., Daddi, E., Illingworth, G. D., Labbé, . I., Moorwood, A., Rix, H., Röttgering, H., Rudnick, G. ., van der Wel, A., van der Werf, P., & van Starkenburg, L. 2003, ApJ, 587, L83
van Dokkum, P. G., Franx, M., Förster Schreiber, . N. M., Illingworth, G. D., Daddi, E., Knudsen, K. K., Labbé, I., Moorwood, A., Rix, H., Röttgering H., Rudnick, G., Trujillo, I., van der Werf, P., van der Wel, A., van Starkenburg, L., & Wuyts, S. 2004, ApJ, 611, 703
Wang, W.-H. and Cowie, L. L. & Barger, A. J. 2004, ApJ, 613, 655
Wilson, J. C., Eikenberry, S. S., Henderson, C. P., Hayward, T. L., Carson, J. C., Pirger, B., Barry, D. J., Brandl, B. R., Houck, J. R., Fitzgerald, G. J., & Stolberg, T. M. 2003, in Instrument Design and Performance for Optical/Infrared Ground-based Telescopes. Edited by Iye, Masanori; Moorwood, Alan F. M. Proceedings of the SPIE, Volume 4841, pp. 451-458 (2003)., 451–458
Yan, H., Dickinson, M., Eisenhardt, P. R. M., Ferguson, H. C., Grogin, N. A., Paolillo, M., Chary, R., Casertano, S., Stern, D., Reach, W. T., Moustakas, L. A., & Fall, S. M. 2004, ApJ, 616, 63